Experimental and theoretical investigation of third-harmonic generation in phase-matched dye solutions

A. PENZKOFER, W. LEUPACHER
*Naturwissenschaftliche Fakultät II — Physik, Universität Regensburg,
D-8400 Regensburg, FRG*

The phase-matched third-harmonic light generation in dye solutions is studied experimentally and theoretically. In the experiments picosecond light pulses of a passive mode-locked Nd–glass laser are converted to the third-harmonic frequency. A third-harmonic conversion efficiency of up to 4×10^{-4} was achieved for one of the dyes investigated (1,3,3,1',3',3'-hexamethylindocarbocyanine iodide in hexafluoroisopropanol). The theoretical calculations determine the influence of various dye and solvent parameters on the conversion efficiency. The conversion efficiency is found to be limited by excited-state absorption of pump laser light and third-harmonic light from the S_1-state to higher singlet states. The S_1-state is mainly populated by two-photon absorption. Amplified spontaneous emission may reduce the limiting effects of excited-state absorption. Phase changes caused by the non-linear refractive index and the refractive index dispersion within the spectral bandwidth of the laser pulses reduce the conversion efficiency. Under ideal conditions conversion efficiencies up to 10% may be achieved.

1. Introduction
Collinear phase-matched and resonantly enhanced third-harmonic light generation is obtainable for some dye solutions with the S_0–S_1 absorption peak between the fundamental and third-harmonic frequency [1–8]. The phase-matching at a certain dye concentration is achieved by the anomalous dispersion of the refractive index of the dye in the S_1-absorption band. The resonant enhancement is due to the S_0–S_1 two-photon resonance.

For nanosecond light pulses of a Nd–YAG laser third-harmonic conversion efficiencies up to 2×10^{-9} have been obtained in the dye 1, 3, 3, 1', 3', 3'-hexamethylindocarbocyanine iodide (HMICI) dissolved in hexafluoroisopropanol (HFIP) [5]. In a recent paper [8] the efficient generation of third-harmonic light with picosecond pump pulses of a mode-locked Nd–glass laser in the dye 1,3,1',3'-tetramethyl-2,2'-dioxopyrimido-6,6'-carbocyanine hydrogen sulphate (PYC) dissolved in HFIP has been studied. A conversion efficiency up to 2×10^{-4} was achieved. The limitations of third-harmonic generation at high pump pulse intensities were analysed by analytical estimates.

In this paper we present experimental results on the third-harmonic generation with picosecond Nd–glass laser pump pulses for the dyes HMICI, PYC and safranine T.

A conversion efficiency up to $\eta \approx 14 \times 10^{-4}$ has been obtained for HMICI in HFIP. The limitations of the energy conversion at high pump pulse intensities for the dyes HMICI, safranine T and PYC are discussed in detail. The measured energy conversion curves are fitted by computer simulations.

The limitations of third-harmonic generation are analysed by numerical calculation. The effects of linear absorption at the third-harmonic frequency, of two-photon absorption, of excited-state absorption at the fundamental and third-harmonic frequency, of S_1-S_0 amplified spontaneous emission, and of phase-mismatch due to the non-linear refractive index and the refractive index dispersion within the spectral pulse bandwidth are included. The analysis indicates that under favourable conditions (extremely weak absorption at third-harmonic frequency) third-harmonic energy conversion efficiencies up to 10% should be achievable for picosecond pump pulses.

For third-harmonic generation in gases a thorough discussion of the limiting processes is given in [9, 10].

2. Experimental results

The third-harmonic generation experiments we carried out with a passively mode-locked Nd–glass laser [11]. The experimental arrangement is shown in Fig. 1. The Nd-phosphate glass laser generates pulses of duration 5 to 6 ps at a wavelength of $\lambda_L = 1.054 \, \mu\text{m}$ (laser glass Hoya LHG5, saturable absorber Kodak dye No. 9860 in 1,2-dichloroethane). A single pulse is selected from the pulse train generated, and is amplified by double passage through an Nd-phosphate glass amplifier (glass: Hoya LHG7). The intensity of the picosecond pulses is determined by transmission measurements through a saturable absorber [12] (photodetectors PD1 and PD2). The two-photon absorption in the dye solutions (sample S) is monitored by transmission measurements with photodetectors PD1 and PD3. The third-harmonic signal is detected by the photomultiplier PM. The third-harmonic energy conversion efficiency is determined by calibrating the photomultiplier PM relative to the photodetector PD1.

The dyes HMICI, PYC and safranine T were investigated. The solvent HFIP ($CF_3-CHOH-CF_3$) was used. The absorption cross-section and stimulated emission cross-section spectra of the dyes at the phase-matching concentration are plotted in Fig. 2 [13, 14]. (For the determination of the absorption spectra see [15], and for the determination of the fluorescence spectra see [16].)
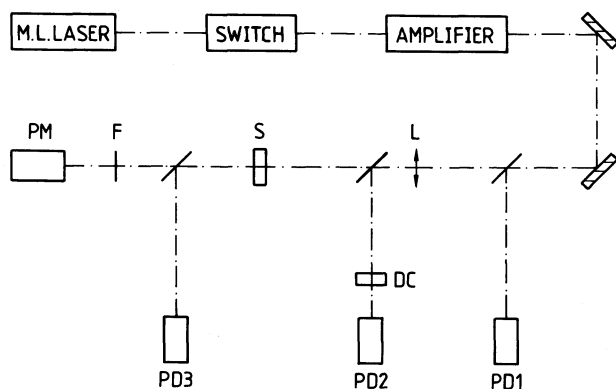

Figure 1 Experimental set-up. PD1 to PD3, photodetectors; DC, saturable absorber cell for intensity detection; L, lens; S, dye sample; F, filters; PM, photomultiplier.
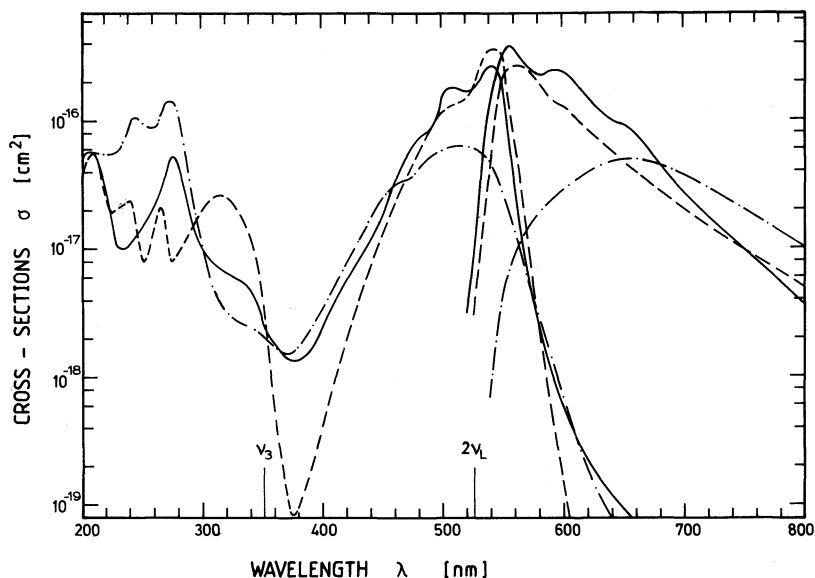
Figure 2 Absorption and emission cross-section spectra of dyes investigated. The spectra are for the phase-matching concentrations of the dyes. Solid curves, HMICI in HFIP; broken curves, PYC in HFIP; chain-broken curves, safranine T in HFIP.
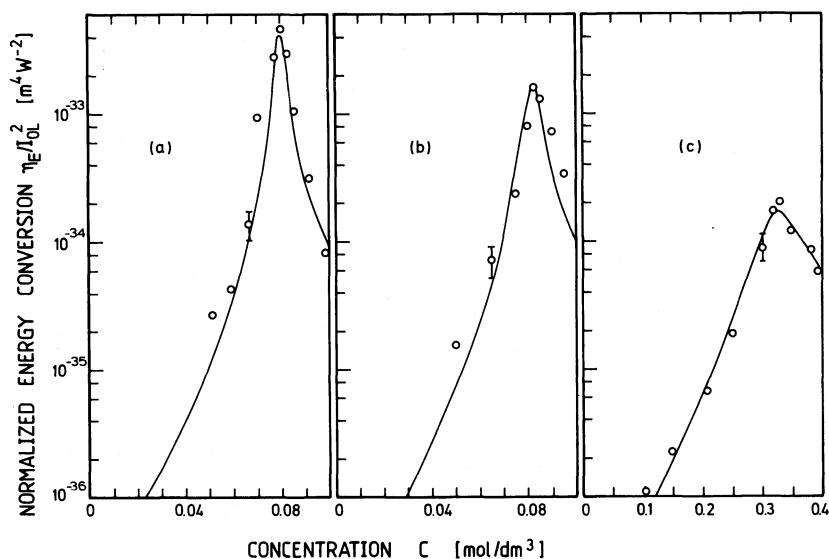

Figure 3 Third-harmonic generation versus dye concentration. Experimental points are obtained for pump pulse peak intensities $I_{0L} \leqslant 4 \times 10^9\,\mathrm{W\,cm^{-2}}$. Curves are calculated for $I_{0L} = 4 \times 10^9\,\mathrm{W\,cm^{-2}}$ by use of Equations 35 and 28 and data from Table I. The wave-vector mismatch Δk (Equation 17) is determined by assuming $n_i^2 - n_{S,i}^2 \propto C$ ($i = $ L,3; $n_{S,i}$ refractive index of solvent; C concentration). (a) HMICI; (b) PYC; (c) safranine T. Solvent: HFIP.
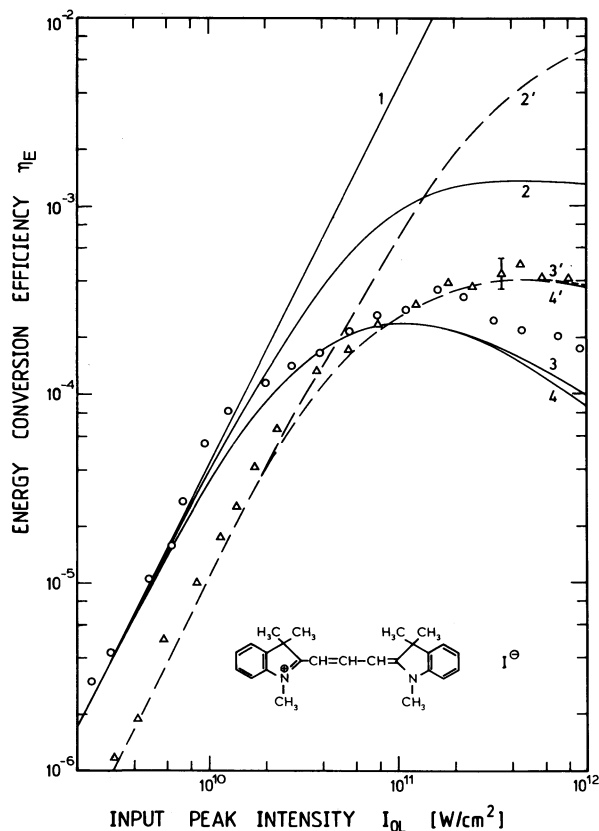
Figure 4 Third-harmonic conversion efficiency versus pump pulse intensity for HMICI in HFIP. Circles and solid curves, sample length $l = 1\,\text{mm}$; triangles and broken curves, $l = 0.1\,\text{mm}$. Curves 3,3' are calculated using the data of Fig. 2 and Table 1. The other curves use the same data except: 1, $\sigma_{LL}^{(2)} = \sigma_{L3}^{(2)} = \sigma_{33}^{(2)} = 0$; 2,2', $\sigma_{ex}^{L} = \sigma_{ex,3} = 0$; 4,4', $\sigma_{em}^{ASE} = 0$. Structural formula of HMICI is included.

The normalized energy conversion η_E/I_{0L}^2 versus dye concentration is shown in Fig. 3 for the three investigated dyes. $\eta_E = W_3(l)/W_L(0)$ is the third-harmonic energy conversion and I_{0L} is the peak intensity of the input laser light. Sample lengths of $l = 1\,\text{mm}$ were used. The pump laser intensity was set to $I_{0L} \lesssim 4 \times 10^9\,\text{W cm}^{-2}$ (no saturation effects). The concentrations of maximum energy conversion are the phase-matching dye concentrations C_{PM} (HMICI, $C_{PM} = 0.08\,\text{mol dm}^{-3}$; PYC, $C_{PM} = 0.0825\,\text{mol dm}^{-3}$; safranine T, $C_{PM} = 0.33\,\text{mol dm}^{-3}$).

The third-harmonic energy conversions versus input pump pulse intensity at the phase-matching dye concentrations are depicted in Figs 4, 5 and 6 for the dyes HMICI, PYC and safranine T, respectively. Dye cell lengths of $l = 1\,\text{mm}$ (circles) and $l = 0.1\,\text{mm}$ (triangles) were used. The energy conversion rises quadratically with input laser peak intensity I_{0L} up to $I_{0L} \approx 2 \times 10^{10}\,\text{W cm}^{-2}$. At higher input intensities the energy conversion rises more slowly and no further increase of energy conversion is observed above $I_{0L} \approx 4 \times 10^{11}\,\text{W cm}^{-2}$.

The theoretical curves in Figs 4 to 6 are explained in Section 4, after a theoretical description of third-harmonic generation in dye solutions in Section 3.

The two-photon absorption cross-sections, $\sigma_{LL}^{(2)}$, for the simultaneous absorptions of two pump laser photons (frequency ν_L) and the S_1-excited state absorption cross-sections σ_{ex}^{L} have been determined previously [14]. The data are listed in Table 1.

TABLE I Spectroscopic data of dyes and solvent investigated. Pulse parameters are $\lambda_L = 1.054\,\mu m$, $\Delta t_L = 5\,ps$, Gaussian shape

Parameter	HFIP	HMICI	PYC	Safranine T	Comments
C_{PM} (mol dm^{-3})	—	0.08	0.0825	0.33	
n_L	1.273	1.292	1.296	1.297	
n_3	1.284	1.292	1.296	1.297	
τ_F (ps)	—	92	9.5	120	[14]
q_F	—	2.7×10^{-2}	2.4×10^{-3}	7.4×10^{-3}	[14]
τ_{FC} (ps)	—	0.7	0.7	0.7	Assumed [31]
τ_{ex} (ps)	—	0.1	0.1	0.1	Assumed [32]
$\tau_{v,6}$ (ps)	—	4	4	4	Assumed [33]
$\tau_{v,7}$ (ps)	—	0.1	0.1	0.1	Assumed
α_L (cm^{-1})	0.07	0.181	0.07	0.263	
σ_3 (cm^2)	0	2.6×10^{-18}	3.55×10^{-18}	2.1×10^{-18}	Fig. 2
σ_{em}^L (cm^2)	0	$\sim 1.5 \times 10^{-19}$	$\sim 7 \times 10^{-20}$	$\sim 2 \times 10^{-19}$	[14][a]
σ_{ex}^{ASE} (cm^2)	0	3×10^{-17}	1×10^{-17}	1×10^{-17}	Assumed
$\sigma_{ex,3}$ (cm^2)	0	1.5×10^{-16}	2.5×10^{-16}	2×10^{-16}	Fitted
σ_{ex}^L (cm^2)	0	4×10^{-17}	2×10^{-17}	7×10^{-18}	[4]
$\sigma_{LL}^{(2)}$ (cm^4 s)	0	2×10^{-49}	1.8×10^{-49}	5×10^{-50}	[14]
$\sigma_{33}^{(2)}$ (cm^4 s)	0	1.8×10^{-48}	1.62×10^{-48}	4.5×10^{-49}	Assumed[b]
$\sigma_{L3}^{(2)}$ (cm^4 s)	0	1.2×10^{-48}	1.08×10^{-48}	3×10^{-49}	Assumed[b]
$n_{2,ij}$	—	—	—	—	c
$\gamma_{xxxx}^{(3)'}(-\omega_3; \omega_L, \omega_L, \omega_L)$ (Cm^4 V^{-4})	1×10^{-62}	1×10^{-62}	1×10^{-62}	1×10^{-62}	[8][d]
$\gamma_{xxxx}^{(3)''}(-\omega_3; \omega_L, \omega_L, \omega_L)$ (Cm^4 V^{-4})	0	2.0×10^{-59}	1.7×10^{-59} [8]	3.3×10^{-60}	d
$\chi_{xxxx}^{(3)'}(-\omega_3; \omega_L, \omega_L, \omega_L)$ (m^2 V^{-2})	1.4×10^{-23}	1.4×10^{-23}	1.4×10^{-23}	1.4×10^{-23}	[8][d]
$\chi_{xxxx}^{(3)''}(-\omega_3; \omega_L, \omega_L, \omega_L)$ (m^2 V^{-2})	0	2.48×10^{-22}	2.0×10^{-22} [8]	1.7×10^{-22}	d
$l_{l,THG}$ (mm)	—	0.24	0.17	0.072	Equation 32

[a] $\sigma_{em}^L = 0$ used in all calculations.

[b] It is assumed that $\chi_{xxxx}^{(3)''}(-\omega_L; \omega_L, -\omega_L, \omega_L) = \chi_{xxxx}^{(3)''}(-\omega_3; \omega_L, -\omega_L, \omega_3) = \chi_{xxxx}^{(3)''}(-\omega_3; \omega_3, -\omega_3, \omega_3)$.

[c] $n_{2,ij}$ ($i = L, 3, j = L, 3$) values are not known. $n_{2,ij} = 0$ is used in calculations except $n_{2,ij}$ values are stated.

[d] Non-linear susceptibility of dyes for third-harmonic generation is assumed to be imaginary, i.e. $\chi_{xxxx,D}^{(3)}(-\omega_3; \omega_L, \omega_L, \omega_L) = -i\chi_{xxxx,D}^{(3)''}(-\omega_3; \omega_L, \omega_L, \omega_L)$ (Equation 18) [7].
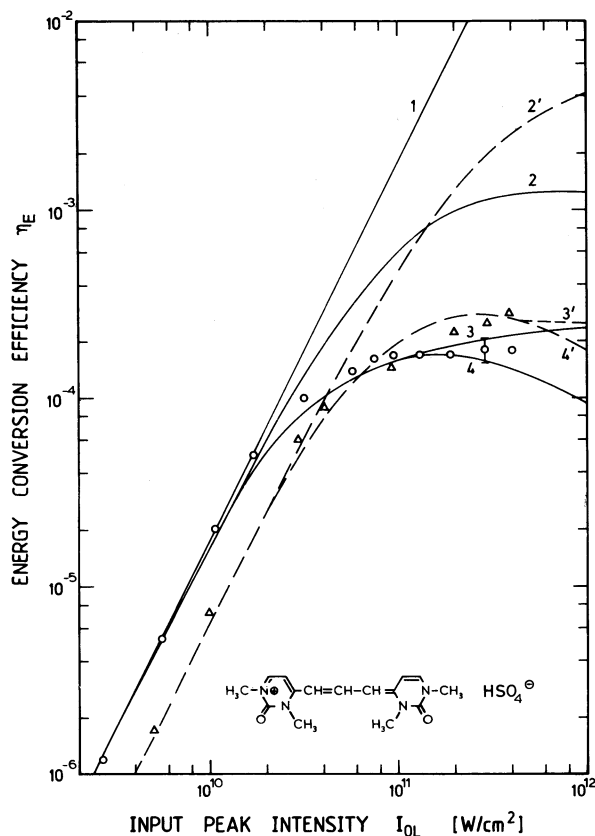
Figure 5 Third-harmonic generation in PYC dissolved in HFIP. Circles and solid curves, sample length $l = 1$ mm; triangles and broken curves, $l = 0.1$ mm. Curve 3,3′ are calculated with the data of Fig. 2 and Table 1. Other curves belong to the same data except: 1, $\sigma_{LL}^{(2)} = \sigma_{L3}^{(2)} = \sigma_{33}^{(2)} = 0$; 2,2′, $\sigma_{ex}^{L} = \sigma_{ex,3} = 0$; 4,4′, $\sigma_{em}^{ASE} = 0$. Structural formula of PYC is included.

3. Theory

In this section a realistic description of third-harmonic generation in dye solutions is presented. The effects include the linear absorption at the fundamental and the third-harmonic frequency, the two-photon absorption of two pump laser photons, the simultaneous absorption of two third-harmonic photons, the two-photon absorption of a pump laser photon and a third-harmonic photon, the excited-state absorption at the fundamental frequency, the excited-state absorption at the third-harmonic frequency, the amplified spontaneous emission and the refractive index changes.

The energy-level system of the dye molecules is presented in Fig. 7. The light absorption and emission processes are included in the figure. A similar level system was used in [14] to describe S_0–S_1 two-photon absorption dynamics in dye solutions. Here the level system is extended to include the third-harmonic generation, the two-photon absorptions of a pump laser and a third-harmonic photon ($\sigma_{L3}^{(2)}$) and of two third-harmonic photons ($\sigma_{33}^{(2)}$), the linear absorption of third-harmonic light (σ_3) and the excited-state absorption of the third-harmonic light ($\sigma_{ex,3}$).

The dynamics of third-harmonic generation, two-photon absorption, ground-state absorption, excited-state absorption, amplified spontaneous emission and phase-modulation are described by the following differential equation system (see also [14]). The equations are transformed to a moving frame by $t' = t - nz/c_0$ and $z' = z$, where t is the time, z the spatial position in the propagation direction, n the refractive index and c_0 the
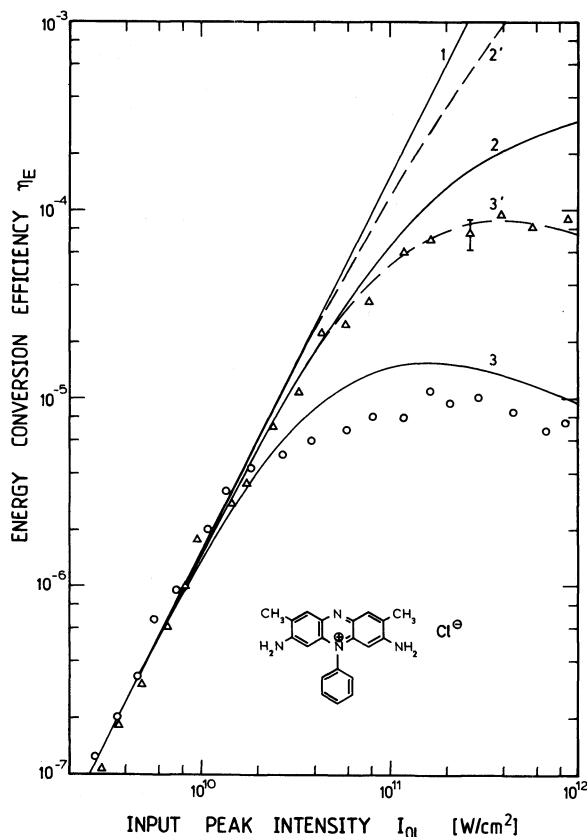
232

Figure 6 Third-harmonic generation for safranine T in HFIP. Circles and solid curves, $l = 1$ mm; triangles and broken curves, $l = 0.1$ mm. Curves 3,3' are calculated with data of Fig. 2 and Table I. Same curves are obtained for $\sigma_{em}^{ASE} = 0$. Curve 1 is for $\sigma_{LL}^{(2)} = \sigma_{L3}^{(2)} = \sigma_{33}^{(2)} = 0$, and curves 2,2' for $\sigma_{ex}^{L} = \sigma_{ex,3} = 0$. Other data are the same as for curves 3 and 3'. Structural formula of safranine T is included.

speed of light *in vacuo*. The equations are

$$\frac{\partial N_1}{\partial t'} = -(N_1 - N_8)\frac{\sigma_3 I_3}{hv_3} - \frac{\sigma_{LL}^{(2)}(N_1 - N_2)}{2(hv_L)^2} I_L^2 - \frac{\sigma_{33}^{(2)}(N_1 - N_{11})}{2(hv_3)^2} I_3^2$$

$$- \frac{\sigma_{L3}^{(2)}(N_1 - N_{10})}{h^2 v_L v_3} I_L I_3 + \sum_{i=1}^{m}(N_3 - N_{6,i})\frac{\sigma_{em,i}^{ASE} I_{ASE,i}}{hv_{ASE,i}} + (N_3 - N_7)\frac{\sigma_{em}^{L} I_L}{hv_L} + \frac{N_3}{\tau_F}$$

$$\tag{1}$$

$$\frac{\partial N_2}{\partial t'} = \frac{\sigma_{LL}^{(2)}(N_1 - N_2)}{2(hv_L)^2} I_L^2 - \left(N_2 - N_4\frac{N_2}{N_2 + N_3}\right)\frac{\sigma_{ex}^{L} I_L}{hv_L} - \frac{N_2}{\tau_{FC}} - \frac{N_2}{\tau_F} \tag{2}$$

$$\frac{\partial N_3}{\partial t'} = \frac{N_2}{\tau_{FC}} - \left(N_3 - N_4\frac{N_3}{N_2 + N_3}\right)\frac{\sigma_{ex}^{L} I_L}{hv_L} - (N_3 - N_5)\frac{\sigma_{ex}^{ASE} I_{ASE}}{hv_{ASE}} - (N_3 - N_9)\frac{\sigma_{ex,3} I_3}{hv_3}$$

$$- \sum_{i=1}^{m}(N_3 - N_{6,i})\frac{\sigma_{em,i}^{ASE} I_{ASE,i}}{hv_{ASE,i}} - (N_3 - N_7)\frac{\sigma_{em}^{L} I_L}{hv_L} - \frac{N_3}{\tau_F} + \frac{N_4}{\tau_{ex}^{L}} + \frac{N_5}{\tau_{ex}^{ASE}} + \frac{N_8}{\tau_{ex}^{3H}}$$

$$+ \frac{N_9}{\tau_{ex,3}} + \frac{N_{10}}{\tau_{ex,10}} + \frac{N_{11}}{\tau_{ex,11}} \tag{3}$$

$$\frac{\partial N_4}{\partial t'} = (N_2 + N_3 - N_4)\frac{\sigma_{ex}^{L} I_L}{hv_L} - \frac{N_4}{\tau_{ex}^{L}} \tag{4}$$
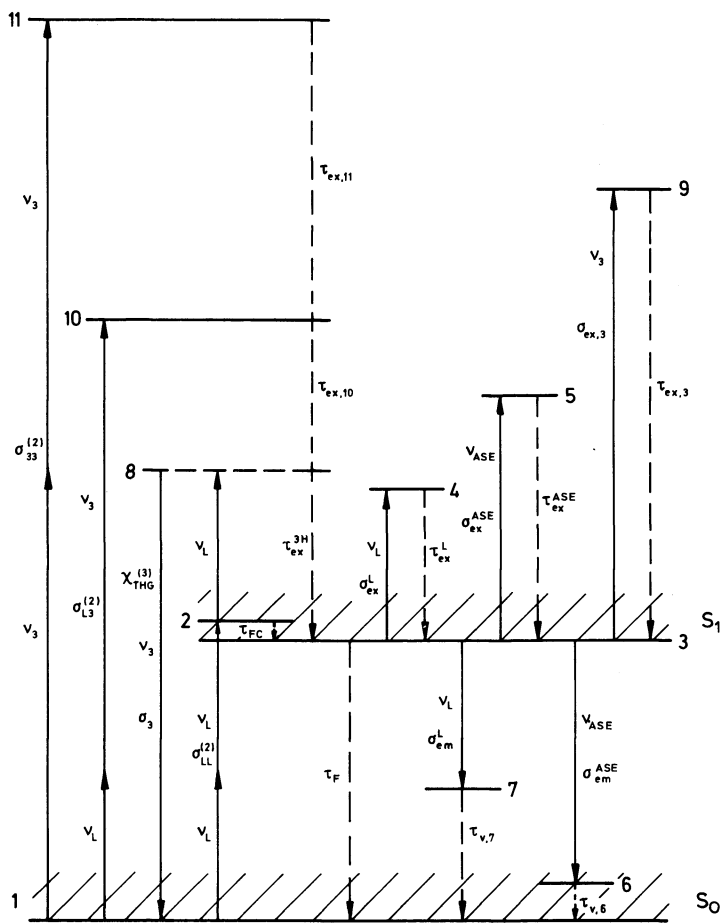
233

Figure 7 Energy-level diagram of dye molecules including the processes of third-harmonic generation, two-photon absorption, excited-state absorption, stimulated emission and amplified spontaneous emission.

$$\frac{\partial N_5}{\partial t'} = (N_3 - N_5) \frac{\sigma_{ex}^{ASE} I_{ASE}}{h\nu_{ASE}} - \frac{N_5}{\tau_{ex}^{ASE}} \tag{5}$$

$$\frac{\partial N_{6,i}}{\partial t'} = \frac{N_3}{\tau_{rad}} e_{ASE,i} + (N_3 - N_{6,i}) \frac{\sigma_{em,i}^{ASE} I_{ASE,i}}{h\nu_{ASE,i}} - \frac{N_{6,i} - \varrho_{6,i} N_1}{\tau_{v,6}} \tag{6}$$

$$\frac{\partial N_7}{\partial t'} = (N_3 - N_7) \frac{\sigma_{em}^{L} I_L}{h\nu_L} - \frac{N_7 - \varrho_7 N_1}{\tau_{v,7}} \tag{7}$$

$$\frac{\partial N_8}{\partial t'} = (N_1 - N_8) \frac{\sigma_3 I_3}{h\nu_3} - \frac{N_8}{\tau_{ex}^{3H}} \tag{8}$$

$$\frac{\partial N_9}{\partial t'} = (N_3 - N_9) \frac{\sigma_{ex,3} I_3}{h\nu_3} - \frac{N_9}{\tau_{ex,3}} \tag{9}$$

$$\frac{\partial N_{10}}{\partial t'} = \frac{\sigma_{L3}^{(2)}(N_1 - N_{10})}{h^2 v_L v_3} I_L I_3 - \frac{N_{10}}{\tau_{ex,10}} \tag{10}$$

$$\frac{\partial N_{11}}{\partial t'} = \frac{\sigma_{33}^{(2)}(N_1 - N_{11})}{2(hv_3)^2} I_3^2 - \frac{N_{11}}{\tau_{ex,11}} \tag{11}$$

$$\frac{\partial I_{ASE,i}}{\partial z'} = e_{ASE,i} \frac{N_3}{\tau_{rad}} h v_{ASE,i} \frac{\Delta\Omega}{4\pi} + (N_3 - N_{6,i})\sigma_{em,i}^{ASE} I_{ASE,i} - (N_3 - N_5)\sigma_{ex}^{ASE} I_{ASE,i} \tag{12}$$

$$\frac{\partial E_{L0}}{\partial z'} = \frac{1}{2}\left(-\sigma_L N_0 - (N_1 - N_2)\frac{\sigma_{LL}^{(2)} I_L}{hv_L} - N_1 \frac{\sigma_{L3}^{(2)} I_3}{hv_3} - (N_2 + N_3 - N_4)\sigma_{ex}^L\right.$$
$$\left. + (N_3 - N_7)\sigma_{em}^L\right) E_{L0} + \frac{i\omega_L}{2n_L c_0}[\chi_{THG}^{(3)*} E_{L0}^2 E_{30}^* \exp(-i\Delta k z') + n_L n_{2,L3}|E_{30}|^2 E_{L0}$$
$$+ n_L n_{2,LL}|E_{L0}|^2 E_{L0}] \tag{13}$$

$$\frac{\partial E_{30}}{\partial z'} = \frac{1}{2}\left(-(N_1 - N_8)\sigma_3 - (N_3 - N_9)\sigma_{ex,3} - N_1 \frac{\sigma_{L3}^{(2)}}{hv_L} I_L - N_1 \frac{\sigma_{33}^{(2)}}{hv_3} I_3\right) E_{30}$$
$$+ \frac{i\omega_3}{2n_3 c_0}[\chi_{THG}^{(3)} E_{L0}^3 \exp(i\Delta k z') + n_L n_{2,L3}|E_{L0}|^2 E_{30} + n_3 n_{2,33}|E_{30}|^2 E_{30}] \tag{14}$$

$$I_L = \frac{n_L \varepsilon_0 c_0}{2}|E_{L0}|^2 \tag{15}$$

$$I_3 = \frac{n_3 \varepsilon_0 c_0}{2}|E_{30}|^2 \tag{16}$$

$$\Delta k = k_3 - 3k_L = \frac{3\omega_L}{c_0}(n_3 - n_L) = \frac{6\pi v_L}{c_0}(n_3 - n_L) = 6\pi\tilde{v}_L(n_3 - n_L) \tag{17}$$

The initial conditions for the number densities of the level populations are $N_1(t' = -\infty, r, z) = N_0$, $N_2(-\infty) = N_3(-\infty) = N_4(-\infty) = N_5(-\infty) = N_8(-\infty) = N_9(-\infty) = N_{10}(-\infty) = N_{11}(-\infty) = 0$, $N_{6,i}(-\infty) = \varrho_{6,i} N_0$ and $N_7(-\infty) = \varrho_7 N_0$. N_0 is the total number density of dye molecules. The terminal level of amplified spontaneous emission (6) is divided into sublevels (6, i) to account for the variations of the thermal level population ($\varrho_{6,i}$) and of the stimulated emission cross-section ($\sigma_{em,i}^{ASE}$) with frequency. The thermal level population factors $\varrho_{6,i}$ and ϱ_7 are approximately given by $\varrho_{6,i} \approx \sigma_A(v_{ASE,i})/\sigma_{em,i}^{ASE}$ and $\varrho_7 \approx \sigma_A(v_L)/\sigma_{em}^L$. $\sigma_A(v_{ASE,i})$ and $\sigma_A(v_L)$ are the apparent absorption cross-sections at $v_{ASE,i}$ and v_L, respectively [17, 18].

The initial light intensities are $I_L(t', r, z = 0) = I_{0L} \exp(-t'/t_0^2) \exp(-r^2/r_0^2)$, $I_{ASE,i}(t', r, z = 0) = 0$ $(i = 1, \ldots, m)$ and $I_3(t', r, z = 0) = 0$. I_{0L} is the input pump pulse peak intensity. $t_0 = \Delta t_L/2[\ln(2)]^{1/2}$ is half the $(1/e)$-pulse width (Δt_L full width at half maximum) and r_0 is the $(1/e)$-beam radius.

Equation 1 describes the population changes of the S_0-band. N_1 comprises the populations of levels 6 and 7. The first term is due to linear absorption of the third-harmonic light. The second term is responsible for two-photon absorption of two pump laser photons (frequency v_L, circular frequency $\omega_L = 2\pi v_L$). The third term gives the two-photon absorption of two third-harmonic photons (frequency v_3, $\omega_3 = 2\pi v_3$) and the fourth term gives the simultaneous absorption of a pump laser photon and a third-harmonic photon. The

fifth term handles the amplified spontaneous emission, and the sixth term gives the stimulated emission at the laser frequency. The last term gives the $S_1 - S_0$ relaxation.

The second equation includes the two-photon absorption, the excited-state absorption, the relaxation within the S_1-band and the relaxation to the S_0-band. The third equation handles the S_1-state dynamics. The various terms describe the level population by Franck–Condon relaxation, the excited-state absorptions at frequencies v_L, v_{ASE} and v_3, the amplified spontaneous emission, the stimulated emission at the pump laser frequency v_L and various relaxation processes.

Equations 4, 5 and 9 describe excited-state absorptions. Equation 6 handles the terminal level populations of the amplified spontaneous emission process. The first term gives the spontaneous emission contribution to the frequency interval $\Delta v_{6,i}$. $e_{ASE,i} = E(v_{ASE,i})\Delta v_{6,i}/q_F$ is the fraction of fluorescence light within the frequency interval $\Delta v_{6,i}$ around $v_{ASE,i}$. $E(v_{ASE,i})$ is the fluorescence quantum distribution ($\int_{em} E(v)\,dv = q_F$, q_F fluorescence quantum efficiency, integration over the $S_1 - S_0$ fluorescence band [16]). The second term of Equation 6 gives the fluorescence light amplification, and the last term causes thermalization within the S_0-band with a time constant $\tau_{v,6}$.

Equation 7 describes the stimulated emission at the pump laser frequency. The first term gives the stimulated emission and the second term causes population thermalization within the S_0-band.

Equation 8 takes care of the population of level 8 by ground-state absorption of the generated third-harmonic light. Equations 10 and 11 handle the populations of levels 10 and 11 by two-photon absorption of photons of frequency v_L and v_3 and of two photons of frequency v_3, respectively, and the relaxation to level 3.

Equation 12 describes the amplification of fluorescence light. The first term gives the seeding spontaneous emission in a frequency interval $\Delta v_{6,i}$ around $v_{ASE,i}$. $\Delta\Omega$ is the solid angle of efficient amplified spontaneous emission. The second term is responsible for amplification of fluorescence light and the third term takes care of excited-state absorption.

Equation 13 describes the changes of the electric field strength of the pump laser. The first term gives linear losses, the second and third terms give two-photon absorption losses ($2\omega_L$ and $\omega_L + \omega_3$), the fourth term is due to excited-state absorption and the fifth term handles the stimulated emission. The sixth term $[\chi_{THG}^{(3)*} = \chi_{xxxx}^{(3)*}(-\omega_3; \omega_L, \omega_L, \omega_L)]$ gives the pump pulse reduction by third-harmonic generation. The seventh term ($n_{2,L3}$) takes care of third-harmonic field-induced phase changes and the last term ($n_{2,LL}$) gives the pump field-induced phase-modulation. $n_{2,L3}$ and $n_{2,LL}$ are non-linear refractive indices. The wave-vector mismatch Δk is given by Equation 17.

The build-up of the third-harmonic light field is described by Equation 14. The first term is due to ground-state absorption and the second term is due to excited-state absorption. The third and fourth terms are due to two-photon absorption losses ($\omega_L + \omega_3$ and $2\omega_3$). The fifth term gives the third-harmonic generation. The sixth and seventh terms ($n_{2,L3}$ and $n_{2,33}$) are due to phase changes caused by the pump pulse and the third-harmonic light, respectively. $n_{2,L3}$ and $n_{2,33}$ are non-linear refractive indices.

The relation between field strength and light intensity is presented by Equations 15 and 16. A derivation of Equations 13 and 14 is given in the Appendix, where relations between the phase-changing susceptibilities and the non-linear refractive indices are also derived.

The third-order non-linear susceptibility, $\chi_{THG}^{(3)}$, responsible for third-harmonic generation is given by $\chi_{THG}^{(3)} = \chi_{xxxx}^{(3)}(-\omega_3; \omega_L, \omega_L, \omega_L) = \chi_{xxxx}^{(3)'}(-\omega_3; \omega_L, \omega_L, \omega_L) - i\chi_{xxxx}^{(3)''}(-\omega_3;$

ω_L, ω_L, ω_L). It is composed of solvent and dye contributions, i.e. [19]

$$\chi^{(3)}_{THG} = \chi^{(3)}_{THG,S} + \chi^{(3)}_{THG,D} \qquad (18)$$

$\chi^{(3)}_{THG,S} = \chi^{(3)}_{THG,S0} N_S / N_{S0}$ is the solvent contribution. N_S is the number density of solvent molecules at dye number density N_0. N_{S0} is the number density of the neat solvent ($N_0 = 0$). $\chi^{(3)}_{THG,S}$ is generally real (no resonant contributions). $\chi^{(3)}_{THG,D}$ is the apparent third-harmonic susceptibility of the dye. It includes intrinsic dye molecule contributions and dye–solvent interaction contributions. If dye aggregation [13, 16, 20] occurs, the dye–dye interaction contributes to $\chi^{(3)}_{THG,D}$ [21]. $\chi^{(3)}_{THG,D}$ may be expressed in terms of apparent hyperpolarizabilities $\gamma^{(3)}_{THG,Dj}$ by [19, 22] (see Appendix)

$$\chi^{(3)}_{THG,D} = \frac{L^{(3)}_{THG}}{\varepsilon_0} (N_1 \gamma^{(3)}_{THG,D1} + N_3 \gamma^{(3)}_{THG,D3}) \simeq \frac{L^{(3)}_{THG}}{\varepsilon_0} N_0 \gamma^{(3)}_{THG,D} \qquad (19)$$

$\gamma^{(3)}_{THG,D1}$ is the apparent hyperpolarizability of dye molecules in the ground state (level 1) and $\gamma^{(3)}_{THG,D3}$ is the apparent hyperpolarizability of dye molecules in the S_1-state (level 3). $L^{(3)}_{THG} = (n_3^2 + 2)(n_L^2 + 2)^3/81$ is the Lorentz local-field correction factor. Since ground-state depletion is weak in the third-harmonic generation process (see Fig. 8), the second equality of Equation 19 is reasonably accurate [$\gamma^{(3)}_{THG,D} \approx \gamma^{(3)}_{THG,D1} = \gamma^{(3)}_{D,xxxx}(-\omega_3; \omega_L, \omega_L, \omega_L)$]. The magnitude of $\chi^{(3)}_{THG} = \chi^{(3)'} - i\chi^{(3)''}$ determines the efficiency of third-harmonic generation. The phase of $\chi^{(3)}_{THG}$ practically does not influence the third-harmonic conversion efficiency.

The relations between the two-photon absorption cross-sections $\sigma^{(2)}_{ij}$ and the imaginary parts of the susceptibilities $\chi^{(3)}_{D,xxxx}(-\omega_i; \omega_j, -\omega_j, \omega_i)$ or the hyperpolarizabilities $\gamma^{(3)}_{D,xxxx}(-\omega_i; \omega_j, -\omega_j, \omega_i)$ are given in the Appendix (Equations A23 to A26).
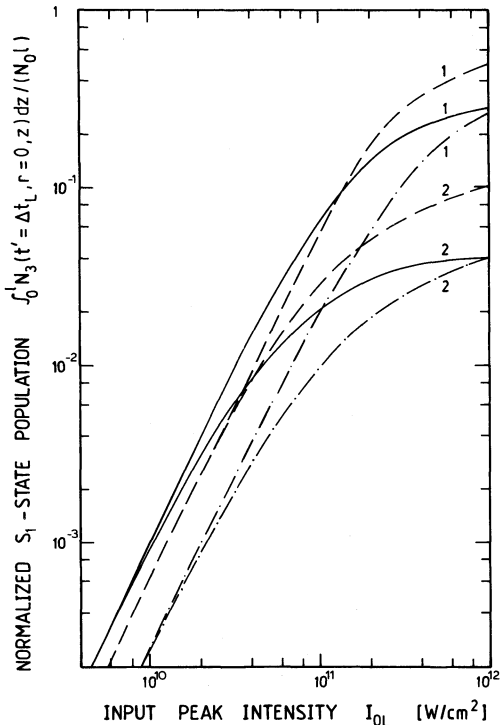

Figure 8 Normalized length-integrated S_1-state populations of dyes investigated. Solid curves, HMICl in HFIP; broken curves, PYC in HFIP; chain-broken curves, safranine T in HFIP. Curves are calculated with data of Table I. Pulse duration $\Delta t_L = 5$ ps. (1) sample length $l = 0.1$ mm; (2) $l = 1$ mm. Dye parameters are listed in Table I.

The relations between the non-linear refractive indices $n_{2,ij}$ and the real parts of the non-linear susceptibilities $\chi_{xxxx}^{(3)}(-\omega_i; \omega_j, -\omega_j, \omega_i)$ are derived in the Appendix (Equations A27 to A30).

The refractive indices, n_i, and the wave-vector mismatch, Δk, change with excited-state level population according to Equations A7 and A18. The change of Δk at high pump pulse intensities due to the population-dependent refractive indices is not explicitly analysed below. Its contribution to phase-mismatch is formally added to the non-linear refractive indices $n_{2,ij}$ (see Figs 19 and 20, below).

The third-harmonic intensity conversion is $\eta_1 = I_3(l)/I_L(0)$. The time-integrated third-harmonic conversion is

$$\eta_{TI} = \int_{-\infty}^{\infty} I_3(t', l) \, dt' / \int_{-\infty}^{\infty} I_L(t', 0) \, dt' \tag{20}$$

Finally, the third-harmonic energy conversion is

$$\eta_E = W_3(l)/W_L(0) = \int_0^{\infty} r \int_{-\infty}^{\infty} I_3(t', r, l) \, dt' \, dr / \int_0^{\infty} r \int_{-\infty}^{\infty} I_L(t', r, 0) \, dt' \, dr \tag{21}$$

At low pump pulse intensities the population changes of the various levels are negligible. A pump pulse depletion does not occur. The effects of two-photon absorption, excited-state absorption and amplified spontaneous emission are diminishingly weak. The whole equation system 1 to 14 reduces to [23]:

$$\frac{\partial E_{L0}}{\partial z'} = -\frac{1}{2} \sigma_L N_0 E_{L0} \tag{22}$$

$$\frac{\partial E_{30}}{\partial z'} = -\frac{1}{2} \sigma_3 N_0 + \frac{i\omega_3}{2n_3 c_0} \chi_{THG}^{(3)} E_{L0}^3 \exp(-i\Delta k z') \tag{23}$$

For $E_{30}(0) = 0$ the solutions of Equations 22 and 23 are given by [23]:

$$E_{L0}(z') = E_{L0}(0) \exp\left(-\frac{1}{2}\sigma_L N_0 z'\right) \tag{24}$$

$$E_{30}(z') = \frac{i\omega_3}{2n_3 c_0} \chi_{THG}^{(3)} E_{L0}^3(0) \exp\left(-\frac{\sigma_3 N_0}{2} z'\right) \frac{\exp\left[\left(\dfrac{\sigma_3 - 3\sigma_L}{2} N_0 - i\Delta k\right) z'\right] - 1}{\dfrac{\sigma_3 - 3\sigma_L}{2} N_0 - i\Delta k} \tag{25}$$

The intensities at $z' = l$ are (Equations 15 and 16) [23]:

$$I_L(l) = I_L(0) \exp(-\sigma_L N_0 l) \tag{26}$$

$$I_3(l) = \kappa_{THG} |\chi_{THG}^{(3)}|^2 I_L^3(0) \tag{27}$$

with

$$\kappa_{THG} = \frac{\omega_3^3 \left[\exp(-3\sigma_L N_0 l) + \exp(-\sigma_3 N_0 l) - 2\exp\left(-\dfrac{\sigma_3 + 3\sigma_L}{2} N_0 l\right) \right] \cos(\Delta k l)}{n_3 n_L^3 c_0^4 \varepsilon_0^2 \left(\dfrac{(\sigma_3 - 3\sigma_L)^2 N_0^2}{4} + \Delta k^2 \right)} \tag{28}$$

Without absorption ($\sigma_L = 0$, $\sigma_3 = 0$) Equation 28 reduces to

$$\kappa_{THG} = \frac{\omega_3^2}{n_3 n_L^3 c_0^4 \varepsilon_0^2} \frac{\sin^2(\Delta k l/2)}{(\Delta k/2)^2} = \kappa_{THG,0} \frac{\sin^2(\Delta k l/2)}{(\Delta k/2)^2} \tag{29}$$

At phase-matching Equation 29 is given by

$$\kappa_{THG} \;=\; \frac{\omega_3^2 l^2}{n_3 n_L^3 c_0^4 \varepsilon_0^2} \;=\; \kappa_{THG,0} l^2 \tag{30}$$

In the case of $\Delta k = 0$, $\alpha_L = 0$ and $\sigma_3 N_0 l \gg 1$, Equation 28 reduces to

$$\kappa_{THG} \;\leqslant\; \frac{\omega_3^2}{n_3 n_L^3 c_0^4 \varepsilon_0^2}\left(\frac{2}{\sigma_3 N_0}\right)^2 \;=\; \kappa_{THG,0}\left(\frac{2}{\sigma_3 N_0}\right)^2 \;. \tag{31}$$

The equality sign is valid for $\sigma_3 N_0 l \to \infty$. Comparison of Equations 31 and 30 indicates that the maximum conversion efficiency in case of absorption at frequency v_3 ($l = \infty$) is equal to the conversion efficiency in a cell of equivalent length $l_{equ} = 2/(\sigma_3 N_0)$ if no absorption is present.

For non-linear media with absorption at the third-harmonic frequency one may define arbitrarily an effective interaction length $l_{l,THG}$ by

$$l_{l,THG} \;=\; \frac{3}{\sigma_3 N_0} \tag{32}$$

At this length 60.35% of the maximum third-harmonic conversion efficiency for $l \to \infty$ are obtained ($\sigma_L = 0$).

The third-harmonic intensity conversion efficiency is

$$\eta_l \;=\; \frac{I_3(l)}{I_L(0)} \;=\; \kappa_{THG}|\chi_{THG}^{(3)}|^2 I_L^2(0) \tag{33}$$

For Gaussian-shaped pump pulses the time-integrated conversion efficiency is

$$\eta_{TI} \;=\; \frac{\kappa_{THG}}{3}\,|\chi_{THG}^{(3)}|^2 I_{0L}^2(0) \tag{34}$$

and the energy conversion efficiency is

$$\eta_E \;=\; \frac{\kappa_{THG}}{3^{3/2}}\,|\chi_{THG}^{(3)}|^2 I_{0L}^2(0) \tag{35}$$

Equation 35 is very useful to determine the third-order non-linear susceptibility of dye solutions by energy conversion efficiency measurements. $\chi_{THG,D}^{(3)}$ (Equation 18) is determined by measuring separately the third-harmonic generation of the solvent. The real and imaginary parts of $\chi_{THG,D}^{(3)} = \chi_{THG,D}^{(3)'} - i\chi_{THG,D}^{(3)''}$ are determined by measuring the third-harmonic energy conversion efficiency as a function of concentration [19].

The complete equation system 1 to 14 has to be solved to similate the third-harmonic generation at high input pump pulse intensities and to analyse the limiting effects to the third-harmonic generation.

4. Simulation of experimental results

The curves in Figs 4 (HMICI), 5 (PYC) and 6 (safranine T) are calculated by use of the absorption and emission curves of Fig. 2, the spectroscopic data of Table 1 and the parameters listed in the figure captions.

The solid curves are for $l = 1\,mm$ while the broken curves are for $l = 0.1\,mm$. The curves 1 neglect two-photon absorption and subsequent excited-state absorption. Equations 35 and 28 are used in the calculations. These curves determine the third-harmonic non-linear susceptibilities $|\chi_{THG}^{(3)}|$ by fitting to the experimental points at intensities

239

$I_{0L} \lesssim 2 \times 10^{10}\,\mathrm{W\,cm^{-2}}$. The energy conversions are reduced by the strong linear ground-state absorption of the generated third-harmonic light (σ_3, short interaction length $l_{l,\mathrm{THG}}$).

The curves 3,3′ represent the best-fitting curves (data listed in Table I). The effects included are the two-photon absorption processes $\omega_L + \omega_L$ ($\sigma_{LL}^{(2)}$ from [14]), $\omega_L + \omega_3$ ($\sigma_{L3}^{(2)}$, here fitted) and $\omega_3 + \omega_3$ ($\sigma_{33}^{(2)}$, assumed, no influence since I_3 is small), the excited-state absorption of pump light (σ_{ex}^L, from [14]) and of third-harmonic light ($\sigma_{ex,3}$, this work) and the amplified spontaneous emission (σ_{em}^{ASE} from Fig. 2, σ_{ex}^{ASE} is assumed from the ground-state absorption spectrum of Fig. 2). The effects of refractive index changes are neglected since they are thought to be negligibly small for the achieved conversion efficiences (see Section 5).

The curves 4,4′ do not include the effect of amplified spontaneous emission (the other parameters are the same as for curves 3,3′). The curves indicate that an optimum pump laser intensiy exists above which the third-harmonic conversion efficiency reduces with increasing pump pulse energy because of dominating excited-state absorption. In case of safranine T the curves 4,4′ coincide with 3,3′, indicating that the influence of amplified spontaneous emission on third-harmonic generation is diminishingly small. In the case of HMICI slightly lower third-harmonic energy conversion efficiencies are calculated at high pump pulse intensities without amplification of spontaneous emission. For the dye PYC the amplification of spontaneous emission is strongest [14]. It hinders a decrease of third-harmonic conversion efficiency at high pump pulse intensities (S_1-state level population is lowered within the pump pulse duration).

For the curves 2,2′ the effects of amplified spontaneous emission and excited-state absorption at ν_L and ν_3 are neglected. Only the effects of two-photon absorption of two pump laser photons ($\sigma_{LL}^{(2)}$, from [14]) and of a pump laser photon and a third-harmonic photon ($\sigma_{L3}^{(2)}$, fitted here) are considered. The simultaneous absorption of two third-harmonic photons is negligibly small because of low third-harmonic conversion efficiency (I_3 small). The curves 2,2′ indicate that the two-photon absorption sets an upper limit of the third-harmonic conversion efficiency at high pump pulse intensities. This upper limit increases with sample length, l, as long as $l < l_{l,\mathrm{THG}}$. For $l > l_{l,\mathrm{THG}}$ (Equation 32) the upper limit of conversion efficiency decreases with sample length (compare curves 2 for $l = 1\,\mathrm{mm}$ with curves 2′ for $l = 0.1\,\mathrm{mm}$).

In Fig. 8 the calculated S_1-state populations are presented for HMICI (solid curves), PYC (broken curves) and safranine T (chain-broken curves). The length-integrated population ($\int_0^l N_3 \mathrm{d}z$) towards the end of the pump pulse duration ($t' = \Delta t_L$) is depicted. The curves 1 belong to $l = 0.1\,\mathrm{mm}$ and the curves 2 to $l = 1\,\mathrm{mm}$ (for details see [14]). The S_1-state population rises quadratically with pump pulse intensity at input intensities below $4 \times 10^{10}\,\mathrm{W\,cm^{-2}}$. At high input pump pulse intensities the S_1-state population levels off with the third-harmonic limiting effects.

5. Influence of various dye parameters

The influence of various dye parameters on the third-harmonic conversion efficiency is studied in the following. In the numerical calculations the parameters of HMICI (Table I and Fig. 2) are used except where otherwise stated.

In Fig. 9 the influence of the linear absorption coefficient, $\alpha_3 = N_0\sigma_3$, on third-harmonic conversion efficiency is investigated. Effects of two-photon absorption ($\sigma_{LL}^{(2)} = \sigma_{L3}^{(2)} = \sigma_{33}^{(2)} = 0$), excited-state absorption ($\sigma_{ex}^L = \sigma_{ex,3} = \sigma_{ex}^{ASE} = 0$), amplified spontaneous emission ($\sigma_{em}^{ASE} = 0$), linear pump laser absorption ($\alpha_L = \sigma_L N_0 = 0$), phase-mismatch ($\Delta k = 0$) and non-linear refractive indices ($n_{2,LL} = n_{2,33} = n_{2,L3} = 0$ for definition see
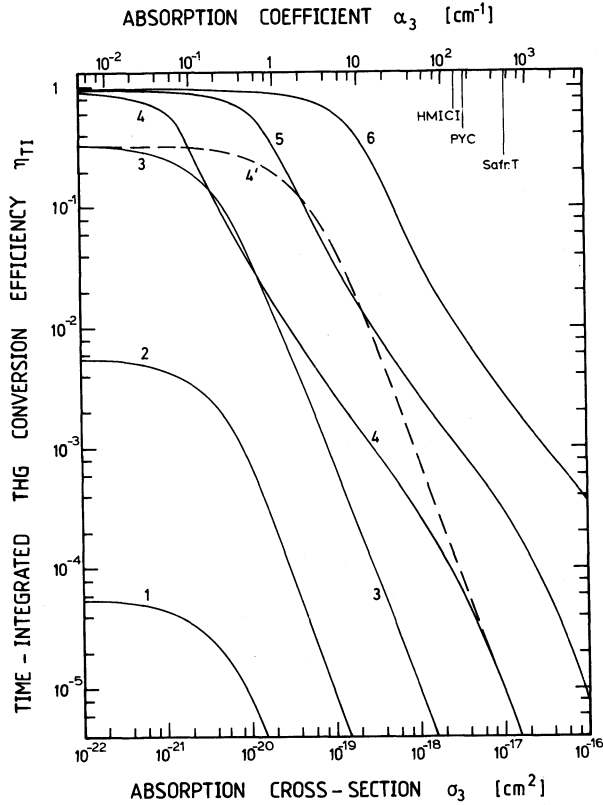
Figure 9 Influence of linear absorption at third-harmonic frequency. HMICl data of Table I are used except $\sigma_{LL}^{(2)} = \sigma_{L3}^{(2)} = \sigma_{33}^{(2)} = 0$, $\alpha_L = 0$, $\sigma_{ex}^L = \sigma_{ex,3} = 0$. The curves are for (1) $I_{0L} = 10^7\,\mathrm{W\,cm^{-2}}$ and $l = 10\,\mathrm{cm}$; (2) $I_{0L} = 10^8\,\mathrm{W\,cm^{-2}}$ and $l = 10\,\mathrm{cm}$; (3) $I_{0L} = 10^9\,\mathrm{W\,cm^{-2}}$ and $l = 10\,\mathrm{cm}$; (4) $I_{0L} = 10^{10}\,\mathrm{W\,cm^{-2}}$ and $l = 10\,\mathrm{cm}$; (4') $I_{0L} = 10^{10}\,\mathrm{W\,cm^{-2}}$ and $l = 1\,\mathrm{cm}$; (5) $I_{0L} = 10^{11}\,\mathrm{W\,cm^{-2}}$ and $l = 1\,\mathrm{cm}$; (6) $I_{0L} = 10^{12}\,\mathrm{W\,cm^{-2}}$ and $l = 1\,\mathrm{mm}$. Absorption coefficients, α_3, of phase-matched solutions of HMICl, PYC and safranine T are indicated

Equations A27 to A29) are excluded. The depicted curves show a strong decrease of third-harmonic conversion efficiency for $l > \alpha_3^{-1}$. Curves 4 ($I_{0L} = 10^{10}\,\mathrm{W\,cm^{-2}}$, $l_1 = 10\,\mathrm{cm}$) and 4' ($I_{0L} = 10^{10}\,\mathrm{W\,cm^{-2}}$, $l_2 = 1\,\mathrm{cm}$) show the influences of sample length and α_3, in the case of pump pulse depletion. In case of $\alpha_3^{-1} > l_1 > l_2$ the conversion efficiency is higher for longer samples. In an intermediate region $l_1 \gtrsim \alpha_3^{-1} \gtrsim l_2$, the shorter sample gives the higher conversion, since in the shorter sample not so much pump light is transferred to the third-harmonic light which is absorbed. For large absorption coefficients $l_1 > l_2 \gg \alpha_3^{-1}$ the conversion efficiences become independent of sample length, since the conversion efficiency becomes very low and pump pulse depletion does not occur.

The reduction of third-harmonic light generation with increasing linear pump pulse absorption is depicted in Fig. 10 ($l = 1\,\mathrm{cm}$). For $l > \alpha_L^{-1}$ the third-harmonic conversion efficiency reduces quadratically with α_L ($\eta \propto I_{0L}^2 l_{eff}^2$, $l_{eff} \propto \alpha_L^{-1}$). The third-harmonic light is generated at the cell entrance before the pump pulse is reduced and it is transferred to the cell exit since no absorption of third-harmonic light is assumed ($\sigma_3 = 0$, $\sigma^{(2)} = 0$, $\sigma_{em}^{ASE} = 0$, $\Delta k = 0$, $n_2 = 0$).

The influence of phase-mismatch is illustrated in Fig. 11. The situation of low pump pulse intensities is depicted where Equations 35 and 28 are applicable. The ratio of the energy conversion envelope in the case of $\Delta k \neq 0$, $\eta_{E,env}(\Delta k)$, to the corresponding energy conversion in the case of $\Delta k = 0$, $\eta_E(0)$, is shown. The ratio is given by

$$\frac{\eta_{E,env}(\Delta k)}{\eta_E(0)} = \min\left(1, \frac{4}{(\Delta kl)^2}\right) \tag{36}$$
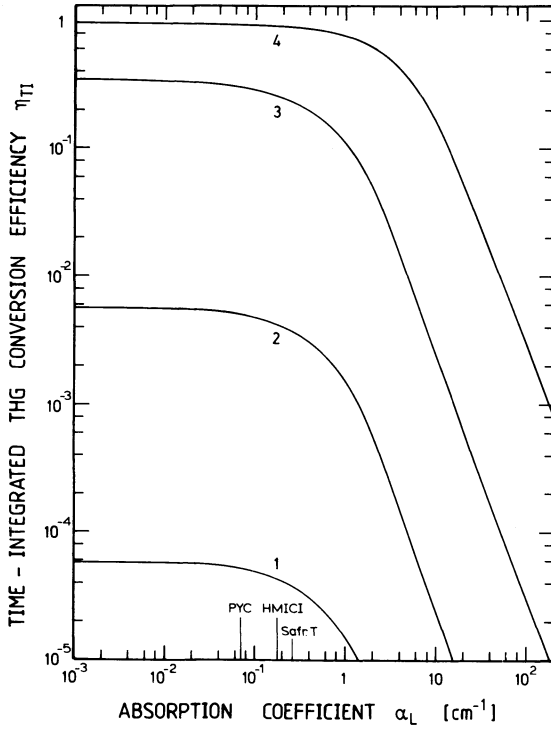
241

Figure 10 Influence of linear absorption of pump laser. HMICl data of Table I are used except $\sigma_{LL}^{(2)} = \sigma_{L3}^{(2)} = \sigma_{33}^{(2)} = 0$, $\sigma_3 = 0$, $\sigma_{ex}^{L} = \sigma_{ex,3} = 0$. Sample length $l = 1$ cm. Curves 1, $I_{0L} = 10^8$ W cm^{-2}; 2, $I_{0L} = 10^9$ W cm^{-2}; 3, $I_{0L} = 10^{10}$ W cm^{-2}; 4, $I_{0L} = 10^{11}$ W cm^{-2}. Absorption coefficients, α_L, of phase-matched solutions of HMICl, PYC and safranine T are indicated.
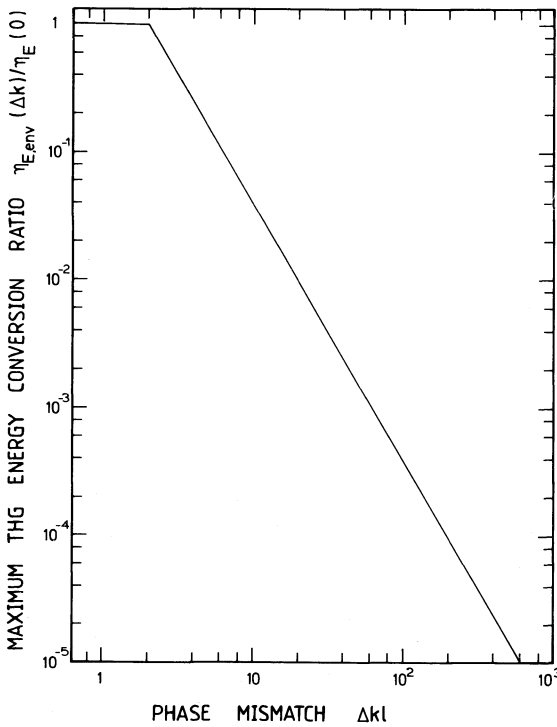

Figure 11 Influence of phase-mismatch on third-harmonic generation. (Equation 36).

$\eta_{E,env}(\Delta k)$ is obtained from Equation 28 by setting $\cos(\Delta kl) = 1$. The wavevector mismatch reduces the effective interaction length to $l_{eff} \approx \Delta k^{-1}$. In some dye solutions with the S_0-S_1 absorption band in the frequency region between v_L and v_3 phase-matching at a certain dye concentration, C_{PM}, is achievable due to the anomalous refractive index dispersion in the wavelength region of the absorption band.

In the presence of absorption of third-harmonic light, σ_3, the energy conversion envelope (Equation 28) becomes proportional to $(\Delta k^2 + \sigma_3^2 N_0^2/4)^{-1}$. The allowed phase-mismatch, Δk, that reduces the energy conversion a factor of 2 is given by

$$\Delta k = \max\left(\frac{\sigma_3 N_0}{2}, \frac{2.78}{l}\right) = \max\left(\frac{\alpha_3}{2}, \frac{2.78}{l}\right) \tag{37}$$

The second part of the maximum condition is obtained from Equations 29 and 30, i.e. $\sin^2(\Delta kl/2)/(\Delta k/2)^2 = l^2/2$. The allowed wave-vector mismatch versus absorption coefficient α_3 is depicted in Fig. 12.

For ultrashort light pulses their spectral widths, $\Delta\tilde{v}_L$ (full width at half maximum), are not negligible. If the phase-matching concentration, C_{PM}, is adjusted to the central frequencies $\tilde{v}_L$ and $\tilde{v}_3$, the spectral wings of the pulses are not phase-matched for third-harmonic generation because of the refractive index dispersion $D = \partial n_3/\partial\tilde{v} - \partial n_L/\partial\tilde{v}$. In the case of phase-matching at the central frequency $\tilde{v}_L$ the phase-mismatch at frequency $\tilde{v}_L = \tilde{v}_L + \delta\tilde{v}_L$ for the process $v_L + v_L + v_L \rightarrow v_3$ is given by $\Delta k(v_L) = 6\pi\tilde{v}_L(n_3 - n_L) = 6\pi\delta\tilde{v}_L\partial[\tilde{v}_L(n_3 - n_L)]/\partial\tilde{v}_L = 6\pi\tilde{v}_L(\partial n_3/\partial\tilde{v}_L - \partial n_L/\partial\tilde{v}_L)\delta\tilde{v}_L = 6\pi\tilde{v}_L D\delta\tilde{v}_L$. The effective phase-mismatch Δk_{eff} due to dispersion is found by integrating over the spectral intensity distribution. For
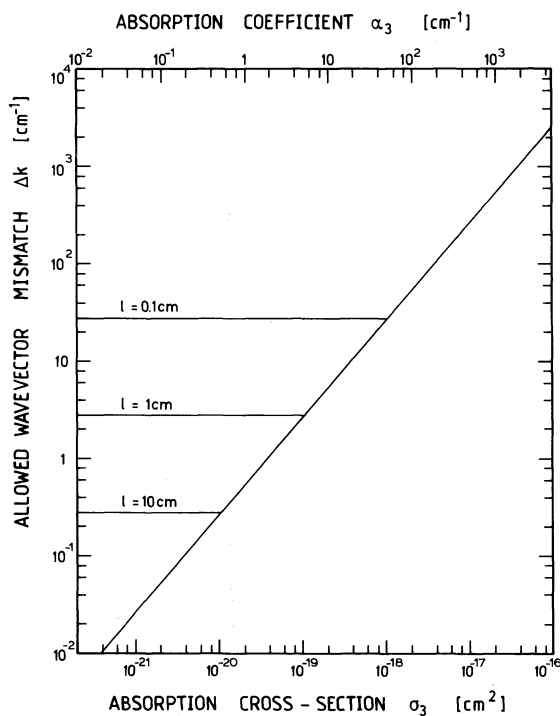

Figure 12 Allowed wave-vector mismatch as a function of sample length and linear absorption cross-section at third-harmonic frequency (Equation 37). The third-harmonic conversion efficiency reduces a factor of 2 compared with $\Delta k = 0$ for the curves shown.

243

Gaussian pulses it is

$$\Delta k_{\text{eff}} = 6\pi\tilde{v}_{\text{L}} D \frac{\int_{-\infty}^{\infty} \delta\tilde{v}_{\text{L}} \exp\left[-4\ln(2)(\delta\tilde{v}_{\text{L}}/\Delta\tilde{v}_{\text{L}})^2\right] \mathrm{d}(\delta\tilde{v}_{\text{L}})}{\int_{-\infty}^{\infty} \exp\left[-4\ln(2)(\delta\tilde{v}_{\text{L}}/\Delta\tilde{v}_{\text{L}})^2\right] \mathrm{d}(\delta\tilde{v}_{\text{L}})} = 3\pi^{1/2}[\ln(2)]^{-1/2}\tilde{v}_{\text{L}} D\Delta\tilde{v}_{\text{L}}$$

$$= \frac{6[\ln(2)]^{1/2}\tilde{v}_{\text{L}} D}{\pi^{1/2}\Delta t_{\text{L}} c_0} \tag{38}$$

The last equality is found by use of the relation $\Delta v_{\text{L}}\Delta t_{\text{L}} = c_0\Delta\tilde{v}_{\text{L}}\Delta t_{\text{L}} = 2\ln(2)\pi^{-1}$ for Fourier transform-limited Gausian pulses [24]. Equation 38 is valid for strict third-harmonic generation $v_{\text{L}} + v_{\text{L}} + v_{\text{L}} \rightarrow v_3$ with $\Delta\tilde{v}_3 = 3\Delta\tilde{v}_{\text{L}}$. For bandwidth-limited pulses frequency mixing processes, $v_{\text{L1}} + v_{\text{L2}} + v_{\text{L3}} \rightarrow v_3$, within the bandwidth Δv_{L} take place and reduce the third-harmonic bandwidth to $\Delta\tilde{v}_3 \approx \Delta v_{\text{L}}$. The effective wave-vector mismatch reduces to

$$\Delta k_{\text{eff}}^{\text{BWL}} \approx \tfrac{1}{3}\Delta k_{\text{eff}} \tag{39}$$

$\Delta k_{\text{eff}}^{\text{BWL}}$ versus dispersion D is plotted in Fig. 13 for the pump pulse durations $\Delta t_{\text{L}} = 10\,\text{ps}$ (1), 1 ps (2), 100 fs (3) and 10 fs (4). For femtosecond pulses the effective phase-mismatch becomes remarkable.

For chirped pulses (due to self-phase modulation [25–29]) the pump pulse frequency changes within the pulse duration and only the strict third-harmonic generation is relevant. In this case the effective wave-vector mismatch is given by Equation 38 (i.e. $\Delta k_{\text{eff}}^{\text{SPM}} = \Delta k_{\text{eff}}$).

The reduction of energy conversion due to refractive index dispersion is illustrated in Fig. 14 for bandwidth-limited pump pulses. $\eta_{\text{E}}(D)/\eta_{\text{E}}(0)$ is depicted versus D for the case of negligible absorption. Equations 35, 29 and 30 are applied, leading to (Gaussian spectral
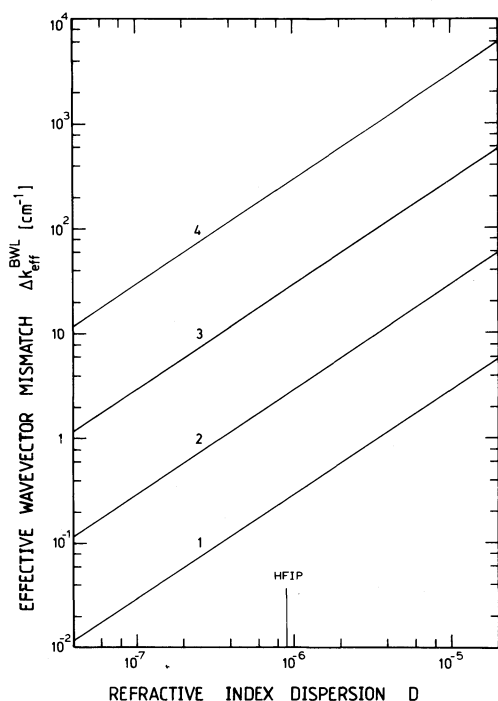

Figure 13 Effective wave-vector mismatch, $\Delta k_{\text{eff}}^{\text{BWL}}$, in third-harmonic generation of ultrashort light pulses phase-matched at centre frequency versus refractive index dispersion, $D = \partial n_3/\partial\tilde{v} - \partial n_{\text{L}}/\partial\tilde{v}$ (Equation 38). Bandwidth-limited Gaussian pulses are assumed. $\lambda_{\text{L}} = \tilde{v}_{\text{L}}^{-1} = 1.054\,\mu\text{m}$. Curves are for the pulse durations (1) $\Delta t_{\text{L}} = 10\,\text{ps}$; (2) 1 ps; (3) 100 fs; (4) 10 fs. In the case of self-phase modulated (chirped) pulses the curves are for (1) $\Delta\tilde{v}_{\text{L}} = 0.5\,\text{cm}^{-1}$; (2) 5 cm^{-1}; (3) 50 cm^{-1}; (4) 500 cm^{-1}. The refractive index dispersion of the solvent HFIP is indicated.

distribution assumed)

$$\frac{\eta_E(D)}{\eta_E(0)} = \frac{\int_{-\infty}^{\infty} \frac{\sin^2(\Delta k l/2)}{\Delta k/2} \exp(-\tilde{v}^2/\tilde{v}_0^2) \, d\tilde{v}}{l^2 \int_{-\infty}^{\infty} \exp(-\tilde{v}^2/\tilde{v}_0^2) \, d\tilde{v}} \tag{40}$$

For bandwidth-limited pulses it is $\Delta k = \Delta k^{\text{BWL}} \frac{1}{3} \Delta k(v_L) = 2\pi \tilde{v}_L D \tilde{v}$ and $\tilde{v}_0 = \Delta \tilde{v}_L / \{2[\ln(2)]^{1/2}\} = \ln(2)^{1/2}/(\pi c_0 \Delta t_L)$. The energy conversion ratio $\eta_E(D)/\eta_E(0)$ depends on $l/\Delta t_L$. The curves depicted belong to various $l/\Delta t_L$ values. For example, curve 4 presents the situation of $l/\Delta t_L = 100 \, \text{cm ps}^{-1}$, i.e. $\Delta t_L = 10 \, \text{fs}$ in the case of $l = 1 \, \text{cm}$. For chirped pulses it is $\Delta k^{\text{SFM}} = \Delta k(v_L) = 6\pi \tilde{v}_L D \tilde{v}$, and $\Delta \tilde{v}_L$ is the spectral bandwidth of the self-phase modulation pulses.

For ultrashort pulses the group velocity dispersion causes a time delay between the third-harmonic light and the pump pulse. It broadens the third-harmonic pulse duration and reduces the conversion efficiency. The reduction of conversion efficiency due to group velocity mismatch is only relevant for bandwidth-limited pulses in long dye cells without absorption (a time delay greater than the pump pulse duration has to occur within the effective interaction length).

The influence of two-photon absorption is analysed in Fig. 15. No excited-state absorption ($\sigma_{\text{ex}}^L = \sigma_{\text{ex},3} = \sigma_{\text{ex}}^{\text{ASE}} = 0$), no linear absorption ($\sigma_L = \sigma_3 = 0$), no amplified spontaneous emission ($\sigma_{\text{em}}^{\text{ASE}} = 0$), no non-linear refractive index effects ($n_{2,\text{LL}} = n_{2,33} = n_{2,\text{L3}} = 0$) and no refractive index dispersion ($D = \partial n_3/\partial \tilde{v} - \partial n_L/\partial \tilde{v} = 0$) are included. For the solid curves, the abscissa is $\sigma^{(2)} = \sigma_{\text{LL}}^{(2)}(\sigma_{\text{L3}}^{(2)} = \sigma_{33}^{(2)} = 0)$. At a fixed $\sigma_{\text{LL}}^{(2)}$-value the
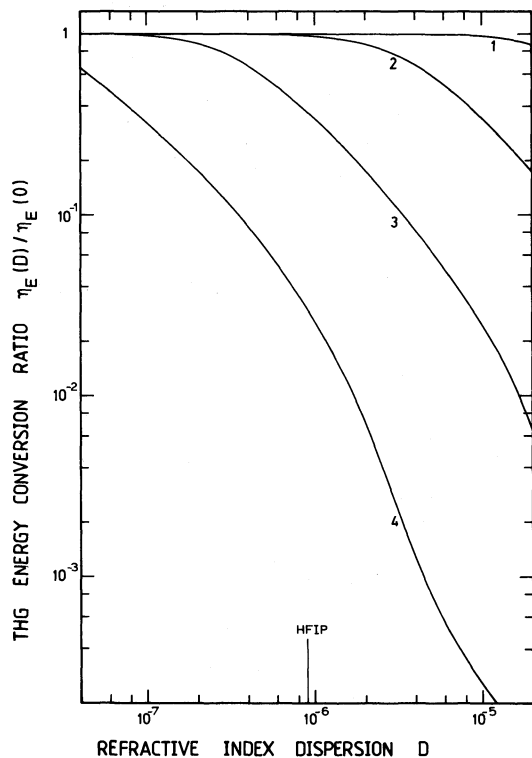

Figure 14 Reduction of third-harmonic conversion efficiency of bandwidth-limited Gaussian pulses versus refractive index dispersion $D = \partial n_3/\partial \tilde{v} - \partial n_L/\partial \tilde{v}$ (Equation 40). The curves are for (1) $l/\Delta t_L = 0.1 \, \text{cm ps}^{-1}$ (e.g. $l = 1 \, \text{cm}$ and $\Delta t_L = 10 \, \text{ps}$), (2) $1 \, \text{cm ps}^{-1}$ (e.g. $l = 1 \, \text{cm}$ and $\Delta t_L = 1 \, \text{ps}$); (3) $10 \, \text{cm ps}^{-1}$ (e.g. $l = 1 \, \text{cm}$ and $\Delta t_L = 100 \, \text{fs}$); (4) $100 \, \text{cm ps}^{-1}$ (e.g. $l = 1 \, \text{cm}$ and $\Delta t_L = 10 \, \text{fs}$). Refractive index dispersion of the solvent HFIP is indicated. $\lambda_L = 1.054 \, \mu\text{m}$.
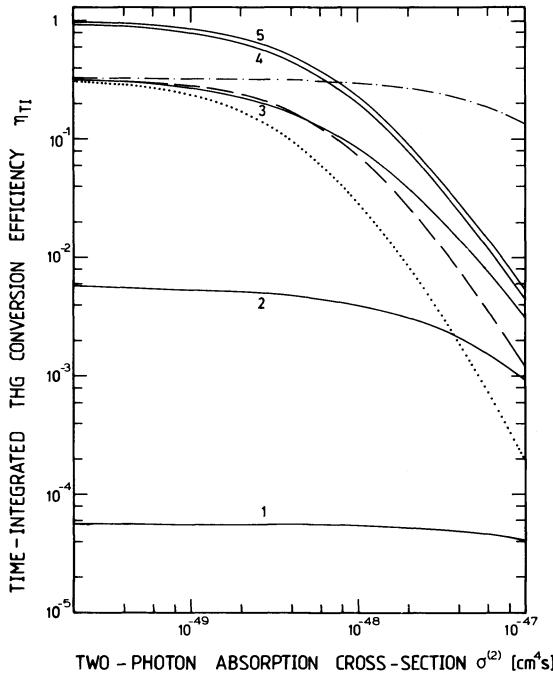
245

Figure 15 Influence of two-photon absorption on third-harmonic generation. Data of HMICl of Table I are used except $\alpha_L = 0$, $\sigma_{ex}^L = \sigma_{ex,3} = 0$, $\sigma_{em}^{ASE} = 0$. For all curves $l = 1$ cm. Solid curves are for $\sigma_{L3}^{(2)} = \sigma_{33}^{(2)} = 0$, abscissa represents $\sigma_{LL}^{(2)}$. (1) $I_{0L} = 10^8$ W cm^{-2}; (2) $I_{0L} = 10^9$ W cm^{-2}; (3) $I_{0L} = 10^{10}$ W cm^{-2}; (4) $I_{0L} = 10^{11}$ W cm^{-2}; (5) $I_{0L} = 10^{12}$ W cm^{-2}. Broken curve $\sigma_{LL}^{(2)} = \sigma_{33}^{(2)} = 0$, abscissa represents $\sigma_{L3}^{(2)}$; $I_{0L} = 10^{10}$ W cm^{-2}. Chain-broken curve, $\sigma_{LL}^{(2)} = \sigma_{L3}^{(2)} = 0$, abscissa represents $\sigma_{33}^{(2)}$, $I_{0L} = 10^{10}$ W cm^{-2}. Dotted curve, $\sigma_{LL}^{(2)} = \sigma_{L3}^{(2)} = \sigma_{33}^{(2)} = \sigma^{(2)}$ (abscissa), $I_{0L} = 10^{10}$ W cm^{-2}.

conversion efficiency approaches a limit with rising pump pulse intensity. For the broken curve the abscissa represents $\sigma^{(2)} = \sigma_{L3}^{(2)}$ ($\sigma_{LL}^{(2)} = \sigma_{33}^{(2)} = 0$, $I_{0L} = 10^{10}$ W cm^{-2}, $l = 1$ cm). The reduction of energy conversion due to the pump laser induced v_3-photon absorption is similar to the reduction of conversion efficiency due to effect of v_L-photon absorption by $\sigma_{LL}^{(2)}$. For the chain-broken curve the abscissa is given by $\sigma^{(2)} = \sigma_{33}^{(2)}$ ($\sigma_{LL}^{(2)} = \sigma_{L3}^{(2)} = 0$). The third-harmonic conversion efficiency is not so strongly reduced, since the third-harmonic intensity, I_3, is lower than the pump laser intensity. The dotted curve shows the cumulative effect of two-photon absorption where $\sigma_{LL}^{(2)} = \sigma_{L3}^{(2)} = \sigma_{33}^{(2)} = \sigma^{(2)}$.

The two-photon absorption populates the first excited singlet state S_1. Starting from the S_1-state, excited-state absorption of the pump laser (σ_{ex}^L) and of the third-harmonic light ($\sigma_{ex,3}$) may drastically reduce the third-harmonic conversion efficiency.

The influence of σ_{ex}^L is illustrated in Fig. 16. Without two-photon absorption ($\sigma_{LL}^{(2)} = \sigma_{L3}^{(2)} = \sigma_{33}^{(2)} = 0$) excited-state absorption of pump laser light does not occur and the conversion efficiency is independent of σ_{ex}^L (the dotted curve is for $I_{0L} = 10^{10}$ W cm^{-2} and $l = 1$ cm). The solid curves in Fig. 16 are for $\sigma_{LL}^{(2)} = 1 \times 10^{-49}$ cm^4 s ($\sigma_{L3}^{(2)} = \sigma_{33}^{(2)} = 0$) and various pump pulse intensities. The broken curves are calculated for $\sigma_{LL}^{(2)} = 8 \times 10^{-49}$ cm^4 s. The crossing of the curves indicates that for a fixed σ_{ex}^L value there exists an optimum pump pulse intensity for maximum third-harmonic conversion efficiency. Increasing the pump pulse intensity above this optimum value results in a reduction of third-harmonic conversion efficiency.

The influence of excited-state absorption of third-harmonic light ($\sigma_{ex,3}$) on the third-harmonic generation is similar to the effect of excited-state absorption of pump laser light (σ_{ex}^L), as is seen by the curves depicted in Fig. 17.

Amplified spontaneous emission contributes to the depopulation of the S_1-state and may reduce the negative influence of excited-state absorption on third-harmonic generation.
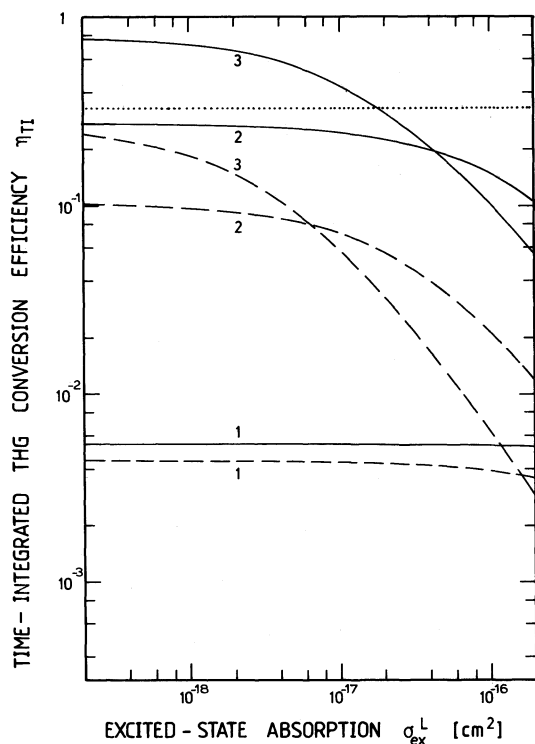
Figure 16 Influence of excited-state absorption of pump laser light on third-harmonic generation. Data of HMICl of Table I are used except $\alpha_L = 0$, $\sigma_{ex,3} = 0$, $\sigma_{em}^{ASE} = 0$, $\sigma_{L3}^{(2)} = \sigma_{33}^{(2)} = 0$. Solid curves, $\sigma_{LL}^{(2)} = 10^{-49}\,cm^4\,s$. Broken curves, $\sigma_{LL}^{(2)} = 8 \times 10^{-49}\,cm^4\,s$. Dotted curve, $\sigma_{LL}^{(2)} = 0$ and $I_{0L} = 10^{10}\,W\,cm^{-2}$. Curves 1, $I_{0L} = 10^9\,W\,cm^{-2}$; 2, $I_{0L} = 10^{10}\,W\,cm^{-2}$; 3, $I_{0L} = 10^{11}\,W\,cm^{-2}$. Sample length $l = 1$ cm for all curves.
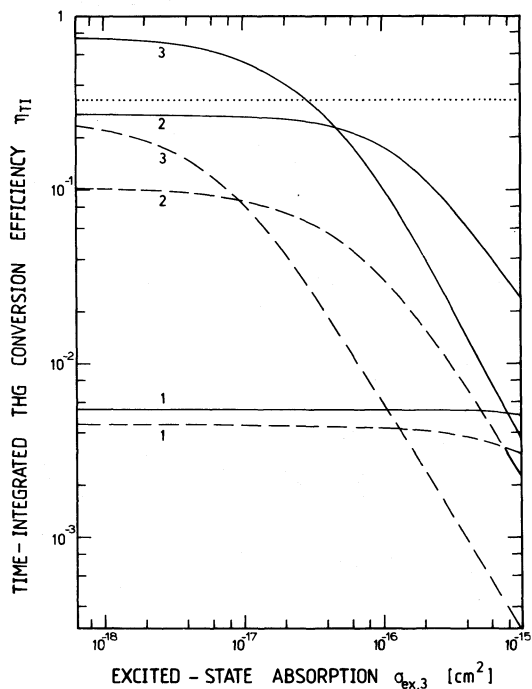

Figure 17 Influence of excited-state absorption at third-harmonic frequency on conversion efficiency. Data of HMICl of Table I are used except $\alpha_L = 0$, $\sigma_{ex}^L = 0$, $\sigma_{em}^{ASE} = 0$, $\sigma_{L3}^{(2)} = \sigma_{33}^{(2)} = 0$. Solid curves, $\sigma_{LL}^{(2)} = 10^{-49}\,cm^4\,s$. Broken curves, $\sigma_{LL}^{(2)} = 8 \times 10^{-49}\,cm^4\,s$. Dotted curve, $\sigma_{LL}^{(2)} = 0$ and $I_{0L} = 10^{10}\,W\,cm^{-2}$. Curves 1, $I_{0L} = 10^9\,W\,cm^{-2}$; 2, $I_{0L} = 10^{10}\,W\,cm^{-2}$; 3, $I_{0L} = 10^{11}\,W\,cm^{-2}$. Samples length $l = 1$ cm for all curves.

247

In Fig. 18 the effect of σ_{em}^{ASE} on third-harmonic conversion efficiency is illustrated. All curves are for $I_{0L} = 10^{11}\,\mathrm{W\,cm^{-2}}$, $\sigma_{LL}^{(2)} = 8 \times 10^{-49}\,\mathrm{cm^4\,s}$ and $l = 1\mathrm{cm}$ ($\sigma_L = \sigma_3 = 0$, $n_2 = 0$, $D = 0$). The solid curves show the time-integrated third-harmonic conversion efficiency $\eta_{TI}(\sigma_{em}^{ASE})$ while the broken curves display the time-integrated amplified spontaneous emission conversion efficiency $\eta_{ASE,TI}(\sigma_{em}^{ASE})$. If $\sigma_{ex,3} = \sigma_{ex}^L = 0$ the third-harmonic generation is not influenced by σ_{em}^{ASE} even in the case of the strong generation of amplified spontaneous emission (curves 5). The broken curve 1 indicates that $\sigma_{ex}^L > 0$ lowers the efficiency of amplified spontaneous emission. For the depicted case of $\sigma_{ex}^L = 2 \times 10^{-16}\,\mathrm{cm^2}$ the third-harmonic conversion efficiency remains independent of σ_{em}^{ASE} (solid curve 1). In the case of $\sigma_{ex}^L = 0$ and $\sigma_{ex,3} > 0$ the occurrence of amplified spontaneous emission increases the third-harmonic conversion efficiency (curves 2, $\sigma_{ex,3} = 2 \times 10^{-16}\,\mathrm{cm^2}$ and $\tau_{v,6} = 4\,\mathrm{ps}$; curves 3, $\sigma_{ex,3} = 2 \times 10^{-16}\,\mathrm{cm^2}$ and $\tau_{v,6} = 1\,\mathrm{ps}$; curves 4, $\sigma_{ex,3} = 2 \times 10^{-16}\,\mathrm{cm^2}$ and $\tau_{v,6} = 0.1\,\mathrm{ps}$). A fast relaxation of the terminal amplified spontaneous emission level (level 6 of Fig. 7) enhances the depopulation of the S_1-state (reduction of bottleneck effect) [14] and increases the efficiency of third-harmonic generation.

Dyes with a fluorescence lifetime τ_F short compared with the pulse duration would depopulate the S_1-state within the pump pulse duration and reduce the effects of excited-state absorption. The behaviour is similar to the situation of strong amplified spontaneous emission.

The population of the S_1-state by two-photon absorption depends on the pump pulse duration. It is accumulative for fluorescence lifetimes longer than the pulse duration. The application of shorter pump pulses would reduce the detrimental effects of excited-state absorption, and the onset of saturation of conversion efficiency would be shifted to higher pump pulse intensities. This allows higher conversion efficiencies for femtosecond pump pulses.
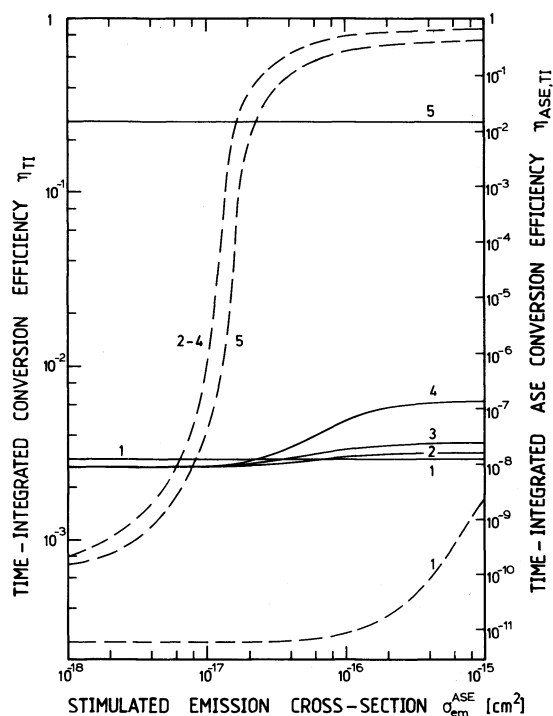

Figure 18 Influence of amplified spontaneous emission on third-harmonic generation. Data of HMICI of Table I are used except $\alpha_L = 0$, $\alpha_{LL}^{(2)} = 8 \times 10^{-49}\,\mathrm{cm^4\,s}$, $\sigma_{L3}^{(2)} = \sigma_{33}^{(2)} = 0$, $\sigma_{ex}^{ASE} = 0$, $\varrho_6 = 5 \times 10^{-4}$, $e_{ASE} = 0.2$. Input pulse peak intensity $I_{0L} = 10^{11}\,\mathrm{W\,cm^{-2}}$. Sample length $l = 1\,\mathrm{cm}$. Solid curves give time-integrated energy conversion efficiency of third harmonic light. The broken curves depict the time-integrated amplified spontaneous emission conversion efficiency. Curves 1, $\sigma_{ex}^L = 1 \times 10^{-16}\,\mathrm{cm^2}$, $\sigma_{ex,3} = 0$, $\tau_{v,6} = 4\,\mathrm{ps}$; 2, $\sigma_{ex}^L = 0$, $\sigma_{ex,3} = 2 \times 10^{-16}\,\mathrm{cm^2}$, $\tau_{v,6} = 4\,\mathrm{ps}$; 3, $\sigma_{ex}^L = 0$, $\sigma_{ex,3} = 2 \times 10^{-16}\,\mathrm{cm^2}$, $\tau_{v,6} = 1\,\mathrm{ps}$; 4, $\sigma_{ex}^L = 0$, $\sigma_{ex,3} = 2 \times 10^{-16}\,\mathrm{cm^2}$, $\tau_{v,6} = 0.1\,\mathrm{ps}$; 5, $\sigma_{ex}^L = \sigma_{ex,3} = 0$, $\tau_{v,6} = 4\,\mathrm{ps}$.

Up to now the influence of the non-linear refractive indices has been neglected. The non-linear refractive indices are defined by Equations A27 to A30. The non-linear refractive indices disturb the phase-matching and therefore reduce the third-harmonic conversion efficiency. The change of the linear refractive indices n_L and n_3 due to level populations (Equation A7) may be included formally in the non-linear refractive indices ($n = \bar{n} + \Delta n + n_2|E|^2 = \bar{n} + n_{2,\text{eff}}|E|^2$).

In Fig. 19 the third-harmonic conversion efficiency versus the non-linear refractive index n_2 is depicted for $\Delta k = 6\pi\tilde{v}_L(n_3 - n_1) = 0$. The non-linear refractive indices are set to $n_{2,\text{LL}} = n_{2,33} = n_2$ and $n_{2,\text{L3}} = 2n_2$. The non-linear refractive indices contribute to the phase-mismatch. For example, the contribution of $n_{2,\text{LL}}$ to the phase-mismatch is approximately given by $\Delta\phi = \Delta n_{\text{LL}}(\omega_L/c_0)l = \frac{1}{2}n_{2,\text{LL}}|E_{0L}|^2(\omega_L/c_0) \; l = n_{2,\text{LL}}I_{0L}\omega_L l/(n_L\varepsilon_0 c_0^2) = 3\chi_{xxxx}^{(3)'}(-\omega_L; \omega_L, -\omega_L, \omega_L)I_{0L}\omega_L l/(n_L^2\varepsilon_0 c_0^2)$ (see Equation A32). For $\Delta\phi > \pi$ a dramatic decrease of the third-harmonic conversion efficiency is observed.

The effect of the non-linear refractive indices n_2 may be compensated to some degree by a certain value of wave-vector mismatch Δk [9]. The phase-mismatch caused by n_2 at the time position $t' = 0$ of maximum pulse intensity is compensated by the linear wave-vector mismatch Δk. This compensation is illustrated in Fig. 20, where the situations of $n_{2,\text{LL}} = n_{2,33} = n_2$ and $n_{2,\text{L3}} = 2n_2$ are shown with $n_2 = 0$ (solid curve), $n_2 = 2.3 \times 10^{-21}\,\text{m}^2\text{V}^{-2}$ (broken curve) and $n_2 = 1.16 \times 10^{-20}\,\text{m}^2\text{V}^{-2}$ (chain-broken curve). The curves are for $I_{0L} = 10^{10}\,\text{W cm}^{-2}$ and $l = 1\,\text{cm}$ ($\alpha_3 = \alpha_L = 0$, $\sigma^{(2)} = 0$).

The illustrated dependence of Figs 9 to 20 indicate various limitations on the third-harmonic conversion efficiencies. Figs 4 to 6 demonstrate the limitations in three real phase-matched dye solutions. In Fig. 21 it is attempted to get a feeling of the maximum
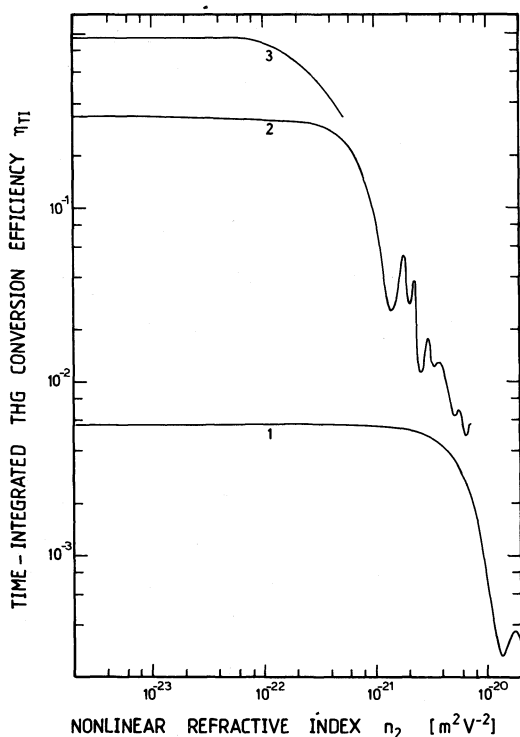

Figure 19 Influence of non-linear refractive indices on third harmonic generation. Data of HMICl of Table I are used except $\alpha_L = 0$, $\sigma_{\text{LL}}^{(2)} = \sigma_{\text{L3}}^{(2)} = \sigma_{33}^{(2)} = 0$, $\sigma_{\text{ex}}^L = \sigma_{\text{ex},3} = 0$, $\sigma_{\text{em}}^{\text{ASE}} = 0$. For n_2 definitions see Equations A27 to A30. Curves are calculated for $n_{2,\text{LL}} = n_{2,33} = n_2$ and $n_{2,\text{L3}} = 2n_2$. $n_L = n_3 = 1.292$. Sample length $l = 1$ cm. Curves 1, $I_{0L} = 10^9\,\text{W cm}^{-2}$; 2, $I_{0L} = 10^{10}\,\text{W cm}^{-2}$; 3, $I_{0L} = 10^{11}\,\text{W cm}^{-2}$.
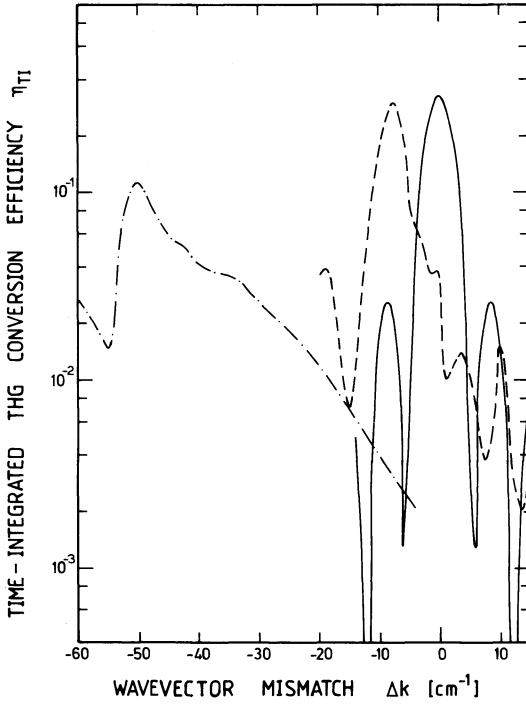
249

Figure 20 Compensation of effects of non-linear refractive indices by wave-vector mismatch. Data of HMICl of Table I are used except $\alpha_L = 0$, $\sigma_{LL}^{(2)} = \sigma_{L3}^{(2)} = \sigma_{33}^{(2)} = 0$, $\sigma_{ex}^L = \sigma_{ex,3} = 0$, $\sigma_{em}^{ASE} = 0$. Sample length $l = 1$ cm. Input peak intensity $I_{0L} = 10^{10}$ W cm^{-2}. The non-linear refractive indices are set to $n_{2,LL} = n_{2,33} = n_2$ and $n_{2,L3} = 2n_2$. Solid curve, $n_2 = 0$; broken curve, $n_2 = 2.3 \times 10^{-21}$ m^2 V^{-2}; chain-broken curve, $n_2 = 1.16 \times 10^{-20}$ m^2 V^{-2}.
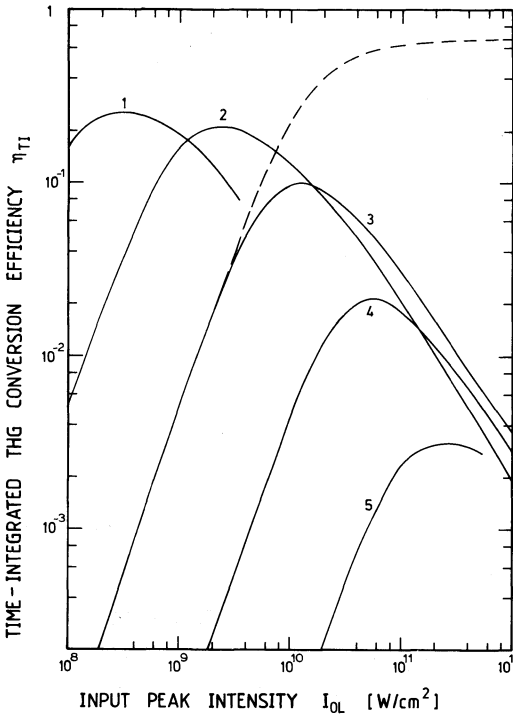

Figure 21 Estimation of possible third-harmonic conversion efficiency versus input pulse peak intensity. Data of HMICl of Table I are used except $\sigma_{em}^{ASE} = 0$, $\sigma_{LL}^{(2)} = \sigma_{L3}^{(2)} = \sigma_{33}^{(2)} = 2 \times 10^{-49}$ cm^4 s, $\sigma_{ex}^L = 2 \times 10^{-17}$ cm^2, $\sigma_{ex,3} = 5 \times 10^{-17}$ cm^2. Curves 1, $l = 100$ cm ($\alpha_L \leqslant \alpha_3 < 0.01$ cm^{-1}); 2, $l = 10$ cm ($\alpha_L \leqslant \alpha_3 < 0.1$ cm^{-1}); 3, $l = 1$ cm ($\alpha_L \leqslant \alpha_3 < 1$ cm^{-1}); 4, $l = 1$ mm ($\alpha_L \leqslant \alpha_3 < 10$ cm^{-1}); 5, $l = 0.1$ mm ($\alpha_L \leqslant \alpha_3 < 100$ cm^{-1}). Broken curve, $l = 1$ cm, $\alpha_{LL}^{(2)} = 2 \times 10^{-49}$ cm^4 s, $\sigma_{L3}^{(2)} = \sigma_{33}^{(2)} = 0$, $\sigma_{ex}^L = \sigma_{ex,3} = 0$.

possible third-harmonic conversion efficiency of picosecond pump pulses in optimum dye solutions. A requirement of high conversion efficiency is low linear absorption at the frequencies ν_L and ν_3. Negligible absorption at the pump laser frequency is given for many dyes. The linear absorption at the third-harmonic frequency hinders high conversion efficiency. Special dyes should be synthesized with very weak cross-sections σ_3 for efficient third-harmonic generation. The larger $\alpha_3 = \sigma_3 N_0$ is, the shorter the effective interaction length $l_{\mathrm{l,THG}} = 3\alpha_3^{-1}$ is. The curves in Fig. 21 are calculated for various sample lengths with $\alpha_3 = 0$. However, these curves also apply reasonably well to the situation of $\alpha_3^{-1} \approx l$. The limiting effect of two-photon absorption cross-section $\sigma_{\mathrm{LL}}^{(2)}$ cannot be avoided, since without a two-photon resonance the third-order non-linear susceptibility for third-harmonic generation would be small. For $\chi_{\mathrm{THG}}^{(3)} = 2.5 \times 10^{-22}\,\mathrm{m^2\,V^{-2}}$ and $\sigma_{\mathrm{LL}}^{(2)} = 2 \times 10^{-49}\,\mathrm{cm^4\,s}$ (data for HMICI) the broken curve in Fig. 21 indicates a limiting conversion efficiency of $\eta_{\mathrm{TI}} \approx 0.7$ for $l = 1\,\mathrm{cm}$, $\sigma_{33}^{(2)} = \sigma_{\mathrm{L3}}^{(2)} = 0$, $\sigma_{\mathrm{ex}}^{\mathrm{L}} = \sigma_{\mathrm{ex,3}} = 0$ ($\alpha_L \ll 1\,\mathrm{cm^{-1}}$, $\alpha_3 < 1\,\mathrm{cm^{-1}}$). The solid curves in Fig. 20 indicate the more realistic situations of $\chi_{\mathrm{THG}}^{(3)} = 2.5 \times 10^{-22}\,\mathrm{m^2\,V^{-2}}$, $\sigma_{\mathrm{LL}}^{(2)} = \sigma_{33}^{(2)} = \sigma_{\mathrm{L3}}^{(2)} = 2 \times 10^{-49}\,\mathrm{cm^4\,s}$, $\sigma_{\mathrm{ex}}^{\mathrm{L}} = 2 \times 10^{-17}\,\mathrm{cm^2}$ and $\sigma_{\mathrm{ex,3}} = 5 \times 10^{-17}\,\mathrm{cm^2}$. In this case a conversion up to $\eta_{\mathrm{TI}} \approx 0.1$ is expected for $l = 1\,\mathrm{cm}$ ($\alpha_L \ll 1\,\mathrm{cm^{-1}}$, $\alpha_3 < 1\,\mathrm{cm^{-1}}$, curve 3). For $l = 0.1\,\mathrm{cm}$ ($\alpha_L \ll 10\,\mathrm{cm^{-1}}$, $\alpha_3 < 10\,\mathrm{cm^{-1}}$) the optimum conversion efficiency would be $\eta_{\mathrm{TI}} \approx 0.02$.

6. Conclusions

In the experimental investigation of efficient third-harmonic generation in dye solutions a conversion efficiency up to 4×10^{-4} has been achieved. For the dyes investigated the relatively high linear absorption coefficient at the third-harmonic frequency results in short effective interaction lengths of $l_{\mathrm{l,THG}} < 0.2\,\mathrm{mm}$ and makes the application of high pump pulse intensities necessary. The conversion efficiency above $10^{11}\,\mathrm{W\,cm^{-2}}$ is limited by the high S_1–S_n excited-state absorption of the generated third-harmonic light. The S_1-state is populated by two-photon absorption of the pump light. The two-photon absorption cannot be avoided because the two-photon resonance increases the third-harmonic susceptibility $\chi_{\mathrm{THG}}^{(3)}$ and makes possible the concentration dependent phase-matching.

The theoretical analysis shows that in dyes with small linear absorption cross-section at the third-harmonic frequency and with small excited-state absorption cross-sections at the pump and the third-harmonic frequency conversions efficiencies up to the 10% region should be possible.

Appendix

The differential equations of the pump laser and third-harmonic laser field (Equations 13 and 14) are derived from Maxwell's equations. One starts with the wave equation in the electric dipole interaction approximation

$$\frac{\partial^2 E}{\partial z^2} - \frac{1}{c_0^2}\frac{\partial^2 E}{\partial t^2} = \mu_0 \frac{\partial^2 P}{\partial t^2} \tag{A1}$$

Inclusion of linear and third-order non-linear effects the polarization is given by

$$P = P_{\mathrm{L}} + P_{\mathrm{NL}} = \varepsilon_0(\chi^{(1)} \cdot E + 4\chi^{(3)} \vdots EEE) \tag{A2}$$

$\chi^{(1)} = \chi^{(1)'} - i\chi^{(1)''}$ is a linear susceptibility tensor of rank 2. It is composed of solvent ($\chi_{\mathrm{S}}^{(1)}$) and solute ($\chi_{\mathrm{D}}^{(1)}$) contributions:

$$\chi^{(1)} = \chi_{\mathrm{S}}^{(1)} + \chi_{\mathrm{D}}^{(1)} = \chi_{\mathrm{S}}^{(1)} + \frac{L^{(1)}}{\varepsilon_0}\sum_{j=1}^{m} N_j \gamma_{\mathrm{D}j}^{(1)} \tag{A3}$$

251

$L^{(1)} = (n^2 + 2)/3$ is the Lorentz local-field correction factor. The N_j are the number densities of the level populations (Fig. 7). $\gamma_{Dj}^{(1)}$ represents the linear polarizability of a dye molecule in level j. $\chi^{(3)} = \chi^{(3)'} - i\chi^{(3)''}$ is a third-order non-linear susceptibility tensor of rank 4. It consists of solvent ($\chi_S^{(3)}$) and solute ($\chi_D^{(3)}$) contributions:

$$\chi^{(3)} = \chi_S^{(3)} + \chi_D^{(3)} = \chi_S^{(3)} + \frac{L^4}{\varepsilon_0} \sum_{j=1}^{m} N_j \gamma_{Dj}^{(3)} \tag{A4}$$

$L^{(4)}$ is the Lorentz local-field correction factor (in the general case $L^{(4)}(\omega_i, \omega_j, \omega_k, \omega_l) = (n_i^2 + 2)(n_j^2 + 2)(n_k^2 + 2)(n_l^2 + 2)/81$). $\gamma_{Dj}^{(3)}$ is the third-order hyperpolarizability of a dye molecule in level j.

Insertion of Equation A2 into A1 gives ($\mu_0 \varepsilon_0 = c_0^{-2}$)

$$\frac{\partial^2 E}{\partial z^2} - \frac{1 + \chi^{(1)}}{c_0^2} \frac{\partial^2 E}{\partial t^2} = \frac{\partial^2 E}{\partial z^2} - \frac{\tilde{n}^2 \partial^2 E}{c_0^2 \partial t^2} = \frac{\partial^2 E}{\partial z^2} - \frac{(n - i\kappa)^2}{c_0^2} \frac{\partial^2 E}{\partial t^2} = \mu_0 \frac{\partial^2 P}{\partial t^2} \tag{A5}$$

where the relation

$$\tilde{n}^2 = (n - i\kappa)^2 = n^2 + \kappa^2 - i2n\kappa = 1 + \chi^{(1)'} - i\chi^{(1)''} \tag{A6}$$

has been used. $\tilde{n}$ is the complex refractive index, n is the real refractive index and κ is the extinction coefficient. Since for the dye solutions $n \gg \kappa$, it is $n = (1 + \chi^{(1)'})^{1/2}$ and $\kappa = \chi^{(1)''}/2n$.

Insertion of Equation A3 into the formula for n gives

$$n = \left(1 + \chi_S^{(1)'} + \frac{L^{(1)}}{\varepsilon_0} \sum_{j=1}^{m} N_j \gamma_{Dj}^{(1)'}\right)^{1/2} = \bar{n} + \Delta n \tag{A7}$$

with $\bar{n} = [1 + \chi_S^{(1)'} + (L^{(1)}/\varepsilon_0) N_0 \gamma_{D1}^{(1)'}]$ representing the refractive index of the unexcited solution. The extinction coefficient is given by

$$\kappa = \frac{1}{2n} \left(\chi_S^{(1)''} + \frac{L^{(1)}}{\varepsilon_0} \sum_{j=1}^{m} N_j \gamma_{Dj}^{(1)''}\right) = \bar{\kappa} + \Delta\kappa \tag{A8}$$

with

$$\bar{\kappa} = \frac{1}{2\bar{n}} \left(\chi_S^{(1)''} + \frac{L^{(1)}}{\varepsilon_0} N_0 \gamma_{D1}^{(1)''}\right)$$

Equation A5 is solved by using the plane-wave ansatz for the third-harmonic generation:

$$E = E_L + E_3 = \tfrac{1}{2}\{E_{L0} \exp[i(\omega_L t - k_L z)] + E_{30} \exp[i(\omega_3 t - k_3 z)] + \text{c.c.}\} \tag{A9}$$

$$P_{NL} = P_{NL,L} + P_{NL,3} = \tfrac{1}{2}\{P_{NL,L0} \exp[i(\omega_L t - k_L z)] + P_{NL,30} \exp[i(\omega_3 t - k_3 z)] + \text{c.c.}\} \tag{A10}$$

with the wavevectors $k_L = n_L \omega_L/c_0 = (\bar{n}_L + \Delta n_L)\omega_L/c_0$ and $k_3 = n_3 \omega_3/c_0 = (\bar{n}_3 + \Delta n_3)\omega_3/c_0$. Insertion of Equations A9 and A10 into A5 gives

$$\left(\frac{\partial^2}{\partial z^2} - k_i^2 - i2k_i \frac{\partial}{\partial z} + \frac{(n_i^2 - i\chi_i^{(1)''})}{c_0^2} \omega_i^2 - \frac{i2(n_i^2 - i\chi_i^{(1)''})}{c_0^2} \omega_i \frac{\partial}{\partial t} - \frac{(n_i^2 - i\chi_i^{(1)''})}{c_0^2} \frac{\partial^2}{\partial t^2}\right) E_{i0}$$

$$= -\mu_0 \omega_i^2 P_{NL,i0} + \mu_0 \frac{\partial^2}{\partial t^2} P_{NL,i0} + i2\mu_0 \omega_i P_{NL,i0} \tag{A11}$$

Using the relation $k_i^2 = n_i^2 \omega_i^2 / c_0^2$ and the slowly varying amplitude approximation

$$\left(\frac{\partial^2}{\partial z^2} \ll k_i \frac{\partial}{\partial z}, \; \omega_i^2 \gg \omega_i \frac{\partial}{\partial t} \gg \frac{\partial^2}{\partial t^2} \right)$$

gives

$$\left(\mathrm{i}2k_i \frac{\partial}{\partial z} + \frac{\mathrm{i}2n_i^2 \omega_i}{c_0^2} \frac{\partial}{\partial t} + \frac{\mathrm{i}\chi_i^{(1)''}}{c_0^2} \omega_i^2 \right) E_{i0} \;=\; \mu_0 \omega_i^2 P_{\mathrm{NL},i0} \tag{A12}$$

or ($k_i = n_i \omega_i / c_0$)

$$\left(\frac{\partial}{\partial z} + \frac{n_i}{c_0} \frac{\partial}{\partial t} + \frac{\chi^{(1)''} \omega_i}{2n_i c_0} \right) E_{i0} \;=\; \frac{-\mathrm{i}\omega_i \mu_0 c_0}{2n_i} P_{\mathrm{NL},i0} \tag{A13}$$

Using the definition

$$\alpha_i \;=\; \frac{\chi^{(1)''} \omega_i}{n_i c_0} \;=\; \frac{2\kappa \omega_i}{c_0} \;=\; 4\pi\kappa\tilde{\nu}_i \tag{A14}$$

and the moving frame transformation $t' = t - (n/c_0)z$ and $z' = z$ gives

$$\frac{\partial}{\partial z'} E_{i0} + \frac{\alpha_i}{2} E_{i0} \;=\; \frac{-\mathrm{i}\omega_i \mu_0 c_0}{2n_i} P_{\mathrm{NL},i0} \tag{A15}$$

For the third-harmonic generation in isotropic media with linearly polarized pump pulses $E_{\mathrm{L}} = (E_{\mathrm{L}x}, 0, 0) = (E_{\mathrm{L}}, 0, 0)$, the non-linear polarizations $P_{\mathrm{NL},i0}$ reduce to $(P_{\mathrm{NL},i0,x}, 0, 0) = (P_{\mathrm{NL},i0}, 0, 0)$. The $P_{\mathrm{NL},i0}$ are given by

$$\begin{aligned}
P_{\mathrm{NL,L0}} \;=\;& 3\varepsilon_0 \chi_{xxxx}^{(3)}(-\omega_{\mathrm{L}}; \omega_3, -\omega_{\mathrm{L}}, -\omega_{\mathrm{L}}) E_{30} E_{\mathrm{L0}}^{*2} \exp\left[-\mathrm{i}(k_3 - 3k_{\mathrm{L}})z' \right] \\
&+ 6\varepsilon_0 \chi_{xxxx}^{(3)}(-\omega_{\mathrm{L}}; \omega_3, -\omega_3, \omega_{\mathrm{L}}) |E_{30}|^2 E_{\mathrm{L0}} \\
&+ 3\varepsilon_0 \chi_{xxxx}^{(3)}(-\omega_{\mathrm{L}}; \omega_{\mathrm{L}}, -\omega_{\mathrm{L}}, \omega_{\mathrm{L}}) |E_{\mathrm{L0}}|^2 E_{\mathrm{L0}}
\end{aligned} \tag{A16}$$

$$\begin{aligned}
P_{\mathrm{NL,30}} \;=\;& \varepsilon_0 \chi_{xxxx}^{(3)}(-\omega_3; \omega_{\mathrm{L}}, \omega_{\mathrm{L}}, \omega_{\mathrm{L}}) E_{\mathrm{L0}}^3 \exp\left[\mathrm{i}(k_3 - 3k_{\mathrm{L}})z' \right] \\
&+ 6\varepsilon_0 \chi_{xxxx}^{(3)}(-\omega_3; \omega_{\mathrm{L}}, -\omega_{\mathrm{L}}, \omega_3) |E_{\mathrm{L0}}|^2 E_{30} \\
&+ 3\varepsilon_0 \chi_{xxxx}^{(3)}(-\omega_3; \omega_3, -\omega_3, \omega_3) |E_{30}|^2 E_{30}
\end{aligned} \tag{A17}$$

Inserting Equations A16 and A17 into Equation A15 and using the relations

$$\Delta k \;=\; k_3 - 3k_{\mathrm{L}} \;=\; \frac{3\omega_{\mathrm{L}}}{c_0}(n_3 - n_{\mathrm{L}}) \;=\; \frac{3\omega_{\mathrm{L}}}{c_0}(\bar{n}_3 - \bar{n}_{\mathrm{L}} + \Delta n_3 - \Delta n_{\mathrm{L}}) \tag{A18}$$

and [29]

$$\chi_{xxxx}^{(3)}(-\omega_{\mathrm{L}}; \omega_3, -\omega_{\mathrm{L}}, -\omega_{\mathrm{L}}) \;=\; \chi_{xxxx}^{(3)*}(-\omega_3; \omega_{\mathrm{L}}, \omega_{\mathrm{L}}, \omega_{\mathrm{L}})$$

gives

$$\begin{aligned}
\frac{\partial}{\partial z'} E_{\mathrm{L0}} \;=\;& -\frac{\alpha_{\mathrm{L}}}{2} E_{\mathrm{L0}} - \frac{\mathrm{i}\omega_{\mathrm{L}}}{2n_{\mathrm{L}} c_0} [3\chi_{xxxx}^{(3)*}(-\omega_3, \omega_{\mathrm{L}}, \omega_{\mathrm{L}}, \omega_{\mathrm{L}}) E_{30} E_{\mathrm{L0}}^{*2} \exp\left(-\mathrm{i}\Delta k z'\right) \\
&+ 6\chi_{xxxx}^{(3)}(-\omega_{\mathrm{L}}; \omega_3, -\omega_3, \omega_{\mathrm{L}}) |E_{30}|^2 E_{\mathrm{L0}} + 3\chi_{xxxx}^{(3)}(-\omega_{\mathrm{L}}; \omega_{\mathrm{L}}, -\omega_{\mathrm{L}}, \omega_{\mathrm{L}}) |E_{\mathrm{L0}}|^2 E_{\mathrm{L0}}]
\end{aligned} \tag{A19}$$

253

$$\frac{\partial}{\partial z'} E_{30} = -\frac{\alpha_3}{2} E_{30} - \frac{i\omega_3}{2n_3 c_0} [\chi_{xxxx}^{(3)}(-\omega_3; \omega_L, \omega_L, \omega_L) E_{L0}^3 \exp(i\Delta k z')$$

$$+ 6\chi_{xxxx}^{(3)}(-\omega_3; \omega_L, -\omega_L, \omega_3)|E_{L0}|^2 E_{30} + 3\chi_{xxxx}^{(3)}(-\omega_3; \omega_3, -\omega_3, \omega_3)|E_{30}|^2 E_{30}]$$

$$(A20)$$

The identity between Equations A19, A20 and Equations 13, 14 is obtained by equating

$$\alpha_L = \frac{\chi^{(1)''}(\omega_L)}{2n_L} = \frac{L^{(1)}(\omega_L)}{2n_L \varepsilon_0} [\gamma_S^{(1)''}(\omega_L) + \sum_{j=1}^{m} N_j \gamma_{Dj}^{(1)''}(\omega_L)]$$

$$= N_0 \sigma_L + (N_2 + N_3 - N_4)\sigma_{ex}^L + (N_7 - N_3)\sigma_{em}^L \qquad (A21)$$

$$\alpha_3 = \frac{\chi^{(1)''}(\omega_3)}{2n_3} = \frac{L^{(1)}(\omega_3)}{2n_3 \varepsilon_0} [\gamma_S^{(1)''}(\omega_3) + \sum_{j=1}^{m} N_j \gamma_{Dj}^{(1)''}(\omega_3)]$$

$$= (N_1 - N_2)\sigma_3 + (N_3 - N_9)\sigma_{ex,3} \qquad (A22)$$

$$\chi_{xxxx}^{(3)''}(-\omega_L; \omega_L, -\omega_L, \omega_L) = \frac{L^{(3)}(\omega_L, \omega_L, \omega_L, \omega_L)}{\varepsilon_0} \sum_{j=1}^{m} N_j \gamma_{xxxx,Dj}^{(3)''}(-\omega_L; \omega_L, -\omega_L, \omega_L)$$

$$= (N_1 - N_2) \frac{n_L^2 c_0^2 \varepsilon_0}{6\hbar \omega_L^2} \sigma_{LL}^{(2)} \qquad (A23)$$

$$\chi_{xxxx}^{(3)''}(-\omega_3; \omega_3, -\omega_3, \omega_3) = \frac{L^{(3)}(\omega_3, \omega_3, \omega_3, \omega_3)}{\varepsilon_0} \sum_{j=1}^{m} N_j \gamma_{xxxx,Dj}^{(3)''}(\omega_3; \omega_3, -\omega_3, \omega_3)$$

$$= N_1 \frac{n_3^2 c_0^2 \varepsilon_0}{6\hbar \omega_3^2} \sigma_{33}^{(2)} \qquad (A24)$$

$$\chi_{xxxx}^{(3)''}(-\omega_L; \omega_3, -\omega_3, \omega_L) = \frac{L^{(3)}(\omega_L, \omega_3, \omega_3, \omega_L)}{\varepsilon_0} \sum_{j=1}^{m} N_j \gamma_{xxxx,Dj}^{(3)''}(-\omega_L; \omega_3, -\omega_3, \omega_L)$$

$$= N_1 \frac{n_L n_3 c_0^2 \varepsilon_0}{12\hbar \omega_L \omega_3} \sigma_{L3}^{(2)} \qquad (A25)$$

$$\chi_{xxxx}^{(3)''}(-\omega_3; \omega_L, -\omega_L, \omega_3) = \chi_{xxxx}^{(3)''}(-\omega_L; \omega_3, -\omega_3, \omega_L) \qquad (A26)$$

$$\chi_{xxxx}^{(3)'}(-\omega_L; \omega_L, -\omega_L, \omega_L) = \frac{L^{(3)}(\omega_L, \omega_L, \omega_L, \omega_L)}{\varepsilon_0} [N_S \gamma_{xxxx,S}^{(3)'}(-\omega_L; \omega_L, -\omega_L, \omega_L)$$

$$+ \sum_{j=1}^{m} N_j \gamma_{xxxx,Dj}^{(3)'}(-\omega_L; \omega_L, -\omega_L, \omega_L)] = \frac{n_L n_{2,LL}}{3}$$

$$(A27)$$

$$\chi_{xxxx}^{(3)'}(-\omega_3; \omega_3, -\omega_3, \omega_3) = \frac{L^{(3)}(\omega_3, \omega_3, \omega_3, \omega_3)}{\varepsilon_0} [N_S \gamma_{xxxx,S}^{(3)'}(-\omega_3; \omega_3, -\omega_3, \omega_3)$$

$$+ \sum_{j=1}^{m} N_j \gamma_{xxxx,Dj}^{(3)'}(-\omega_3; \omega_3, -\omega_3, \omega_3)] = \frac{n_3 n_{2,33}}{3}$$

$$(A28)$$

$$\chi^{(3)'}_{xxxx}(-\omega_L; \omega_3, -\omega_3, \omega_L) = \frac{L^{(3)}(\omega_L, \omega_3, \omega_3, \omega_L)}{\varepsilon_0} [N_S \gamma^{(3)'}_{xxxx,S}(-\omega_L; \omega_3, -\omega_3, \omega_L)$$

$$+ \sum_{j=1}^{m} N_j \gamma^{(3)'}_{xxxx,Dj}(-\omega_L; \omega_3, -\omega_3, \omega_L)] = \frac{n_L n_{2,L3}}{6}$$

$$\text{(A29)}$$

$$\chi^{(3)'}_{xxxx}(-\omega_L; \omega_3, -\omega_3, \omega_L) = \chi^{(3)'}_{xxxx}(-\omega_3; \omega_L, -\omega_L, \omega_3) = \frac{n_3 n_{2,3L}}{6} = \frac{n_L n_{2,L3}}{6}$$

$$\text{(A30)}$$

$$\chi^{(3)}_{xxxx}(-\omega_3; \omega_L, \omega_L, \omega_L) = \chi^{(3)*}_{xxxx}(-\omega_L, \omega_3, -\omega_L, -\omega_L) = \chi^{(3)}_{THG} \qquad \text{(A31)}$$

The relations between the non-linear refractive indices and the third-order non-linear susceptibilities are obtained by transferring the terms $-(3\omega_i^2/c_0^2)\, \chi^{(3)'}_{xxxx}(-\omega_i; \omega_i, -\omega_i, \omega_i)|E_{i0}|^2 E_{i0} - (6\omega_i^2/c_0^2)\, \chi^{(3)'}_{xxxx}(-\omega_i; \omega_j, -\omega_j, \omega_i)|E_{j0}|^2 E_{i0}$ from the right-hand side of Equation A11 ($P_{NL,i}$ is given by Equations A16 and A17) to the left-hand side of Equation A11 and including them into the fourth term by replacing n_i^2 by

$$(n_i + \Delta n_{ii} + \Delta n_{ij})^2 = (n_i + \tfrac{1}{2}n_{2,ii}|E_{i0}|^2 + \tfrac{1}{2}n_{2,ij}|E_{j0}|^2)^2 \approx n_i^2 + n_i n_{2,ii}|E_{i0}|^2 + n_i n_{2,ij}|E_{j0}|^2$$

$$\text{(A32)}$$

Acknowledgements

References

1. P. P. BEY, J. F. GIULIANI and H. RABIN, *Phys. Rev. Lett.* **19** (1967) 819.
2. P. P. BEY, J. F. GIULIANI and H. RABIN, *IEEE J. Quantum Electron.* **QE-4** (1968) 932.
3. R. K. CHANG and L. K. GALBRAITH, *Phys. Rev.* **171** (1968) 993.
4. P. P. BEY, J. F. GUILIANI and H. RABIN, *IEEE J. Quantum Electron.* **QE-7** (1971) 86.
5. J. C. DIELS and F. P. SCHÄFER, *Appl. Phys.* **5** (1974) 197.
6. L. I. AL'PEROVICH, T. B. BAVAEV and V. V. SHABALOV, *Soviet J. Appl. Spectrosc.* **26** (1977) 196.
7. W. LEUPACHER and A. PENZKOFER, *Appl. Phys.* **B36** (1985) 25.
8. W. LEUPACHER, A. PENZKOFER, B. RUNDE and K. H. DREXHAGE, *ibid.* **B44** (1987) 133.
9. J. F. REINTJES, 'Nonlinear Parametric Processes in Liquids and Gases' (Academic Press, Orlando, 1984) p. 240.
10. J. F. REINTJES, in 'Laser Handbook', Volume 5, edited by M. Bass and M. L. Stitch (North-Holland, Amsterdam, 1985) Ch. 1.
11. A. PENZKOFER and F. GRAF, *Opt. Quantum Electron.* **17** (1985) 219.
12. A. PENZKOFER, D. VON DER LINDE and A. LAUBEREAU, *Opt. Commun.* **4** (1972) 377.
13. A. PENZKOFER, W. LEUPACHER, B. MEIER, B. RUNDE and K. H. DREXHAGE, *Chem. Phys.* **115** (1987) 143.
14. A. PENZKOFER and W. LEUPACHER, *Opt. Quantum Electron.* **19** (1987) 327.
15. Y. LU and A. PENZKOFER, *Appl. Opt.* **25** (1986) 221.
16. A. PENZKOFER and W. LEUPACHER, *J. Lumin.* **37** (1987) 61.
17. W. BLAU, W. DANKESREITER and A. PENZKOFER, *Chem. Phys.* **85** (1984) 473.
18. A. PENZKOFER and P. SPERBER, *ibid.* **88** (1984) 309.
19. W. LEUPACHER and A. PENZKOFER, *Appl. Phys.* **B36** (1985) 25.

20. Y. LU and A. PENZKOFER, *Chem. Phys.* **107** (1986) 175.
21. A. PENZKOFER, J. SCHMAILZL and H. GLAS, *Appl. Phys.* **B29** (1982) 37.
22. R. W. MINCK, R. W. TERHUNE and C. C. WANG, *Appl. Opt.* **5** (1966) 1595.
23. M. THALHAMMER and A. PENZKOFER, *Appl. Phys.* **B32** (1983) 137.
24. E. P. IPPEN and C. V. SHANK, in 'Ultrashort Light Pulses', edited by S. L. Shapiro. Topics in Applied Physics, Volume 18 (Springer-Verlag, Berlin, 1977) p. 83.
25. F. SHIMIZU, *Phys. Rev. Lett.* **19** (1967) 1097.
26. T. K. GUSTAFSON, J. P. TARAN, H. A. HAUS, J. R. LIFSHITZ and P. L. KELLY, *Phys. Rev.* **177** (1969) 306.
27. S. A. AKHMANOV, R. V. KHOKHLOV and A. P. SUKHORUKOV, in 'Laser Handbook', Volume 2, edited by F. T. Arrecchi and E. O. Schultz-Dubois (North-Holland, Amsterdam, 1972) Ch. E3.
28. R. C. ECKARDT, C. H. LEE and J. N. BRADFORD, *Opto-Electronics* **6** (1974) 67.
29. O. SVELTO, *Prog. Opt.* **12** (1974) 1.
30. P. N. BUTCHER, Nonlinear Optical Phenomena, Bulletin 200, Engineering Experiment Station, Ohio State University (Columbus, Ohio, 1965).
31. A. PENZKOFER, W. FALKENSTEIN and W. KAISER, *Chem. Phys. Lett.* **44** (1976) 82.
32. W. FALKENSTEIN, A. PENZKOFER and W. KAISER, *Opt. Commun.* **27** (1978) 151.
33. D. RICARD and J. DUCUING, *J. Chem. Phys.* **62** (1975) 3616.